Altering the redox status of *Chlamydia trachomatis* directly impacts its developmental cycle progression

Vandana Singh and Scot P. Ouellette*

Department of Pathology, Microbiology, and Immunology, College of Medicine, University of Nebraska Medical Center, Omaha, NE 68198

*Correspondence: scot.ouellette@unmc.edu

Keywords: *Chlamydia*, Alkyl hydroperoxide reductase subunit C (AhpC), CRISPRi, Differentiation, Development, Oxidative stress, Peroxides, Reactive oxygen species (ROS), ROS scavengers

ABSTRACT

Chlamydia trachomatis is an obligate intracellular bacterial pathogen with a unique developmental cycle. It differentiates between two functional and morphological forms: elementary body (EB) and reticulate body (RB). The signals that trigger differentiation from one form to the other are unknown. EBs and RBs have distinctive characteristics that distinguish them, including their size, infectivity, proteome, and transcriptome. Intriguingly, they also differ in their overall redox status as EBs are oxidized and RBs are reduced. We hypothesize that alterations in redox may serve as a trigger for secondary differentiation. To test this, we examined the function of the primary antioxidant enzyme alkyl hydroperoxide reductase subunit C (AhpC), a well-known member of the peroxiredoxins family, in chlamydial growth and development. Based on our hypothesis, we predicted that altering the expression of *ahpC* will modulate chlamydial redox status and trigger earlier or delayed secondary differentiation. To test this, we created *ahpC* overexpression and knockdown strains. During *ahpC* knockdown, ROS levels were elevated, and the bacteria were sensitive to a broad set of peroxide stresses. Interestingly, we observed increased expression of EB-associated genes and concurrent higher production of EBs at an earlier time in the developmental cycle, indicating earlier secondary differentiation occurs under elevated oxidation conditions. In contrast, overexpression of AhpC created a resistant phenotype against oxidizing agents and delayed secondary differentiation. Together, these results indicate that redox potential is a critical factor in developmental cycle progression. For the first time, our study provides a mechanism of chlamydial secondary differentiation dependent on redox status.

Word count: 250

INTRODUCTION

All organisms that are exposed to oxygen are necessarily subjected to oxidative stress. Specifically, the process of metabolizing substrates in the presence of oxygen can generate reactive oxygen species (ROS), which are toxic at high enough concentrations. Thus, from bacteria to humans, systems have evolved to mitigate the accumulation of ROS. At the same time, host defense mechanisms have evolved to leverage ROS production as a means of limiting pathogen growth and survival. Not surprisingly, pathogens have co-evolved to resist these defense mechanisms. For example, many pathogens possess a variety of antioxidant enzymes, such as catalases, glutathione peroxidases, and peroxiredoxins, that help them both subvert ROS-mediated immune system assaults and mitigate metabolic ROS byproducts (Staerck et al., 2017; Wan et al., 2021).

Chlamydia is an obligate intracellular bacterium that has significantly reduced its genome size and content in adapting to obligate host dependence. *Chlamydia trachomatis*, the leading cause of bacterial sexually transmitted diseases and preventable infectious blindness, lacks homologs to catalases or glutathione peroxidases but does possess a homolog of Alkyl hydroperoxide reductase subunit C (AhpC). AhpC is a well-known member of the peroxiredoxins family and is widely conserved in prokaryotes (de Oliveira et al., 2021). Peroxiredoxins can scavenge hydrogen peroxide, peroxynitrite, and organic hydroperoxides (Parsonage et al., 2008; Poole & Ellis, 1996; Seaver & Imlay, 2001) and act as the primary scavenger in pathogens that lack both catalase and glutathione peroxidases (Mastronicola et al., 2014; Richard et al., 2011). Several studies from other bacterial systems have shown that AhpC has a significant role in ROS and RNI scavenging, virulence, and persistence (Cosgrove et al., 2007; Kimura et al., 2012; Oh & Jeon, 2014), and deletion of AhpC creates highly oxidized conditions within the bacterium (Zhang et al., 2019). However, the function of AhpC in chlamydial biology has not been characterized.

Chlamydia is unique among pathogens in undergoing a complex developmental cycle that comprises two distinct morphological forms, the elementary body (EB) and reticulate body (RB) (Abdelrahman & Belland, 2005). The EB is the smaller (~0.3 μm), infectious, and non-dividing form capable of infecting susceptible host cells. Once internalized into a host-derived vacuole termed an inclusion, the EB differentiates into the non-infectious, larger (~1 μm), and replicating RB - this process is known as primary differentiation and represents the early phase of the developmental cycle (Clifton et al., 2005). RBs replicate within the inclusion in the mid-cycle phase using an asymmetric, MreB-dependent polarized division process (Abdelrahman et al., 2016; Lee et al., 2020; Ouellette et al., 2022; Ouellette et al., 2020). In the late phase of the developmental cycle, RBs asynchronously condense into EBs, and this process is termed secondary differentiation. Despite these well-defined differences between chlamydial morphological forms, how *Chlamydia* mechanistically differentiates between functional forms remains unclear.

Intriguingly, a recent study evaluated the redox potential of *Chlamydia* and demonstrated that RBs are reduced, whereas EBs are oxidized (Wang et al., 2014). This is consistent with earlier studies that revealed differences in the crosslinking of outer membrane proteins and type III secretion-related proteins in chlamydial developmental forms (Betts-Hampikian & Fields, 2011; Caldwell et al., 1981; Everett & Hatch, 1995; Wang et al., 2014). Taken together, these observations indicate that, during the developmental cycle, the redox potential of the bacteria is changing. However, whether redox changes in the bacteria directly affect developmental cycle progression is not characterized. Based on the different redox status of the chlamydial developmental forms, we hypothesized that increasing the oxidation of the RB drives secondary differentiation to the EB. We used chlamydial transformants designed to overexpress or reduce AhpC levels to explore the effects of altered redox potential in chlamydial growth and development to test this hypothesis. This study establishes the role of AhpC as an antioxidant in

102 *Chlamydia,* as demonstrated by its ability to counteract different peroxide stresses when
103 overexpressed. Overexpression of AhpC had no negative effect on bacterial replication but
104 delayed the differentiation of RBs to EBs. In contrast, under conditions of *ahpC* knockdown, the
105 organism was highly sensitive to oxidizing conditions. Interestingly, this change in redox
106 potential caused earlier expression of EB-associated (late) genes and production of EBs,
107 leading to a shift in developmental cycle progression. This earlier activation of gene expression
108 related to secondary differentiation in *ahpC* knockdown was also observed when developmental
109 cycle progression was blocked by penicillin treatment. Taken together these data provide
110 mechanistic insight into chlamydial secondary differentiation and are the first to demonstrate
111 redox-regulated differentiation in *Chlamydia*.
112

RESULTS

The redox threshold hypothesis and chlamydial secondary differentiation

The chlamydial EB and RB developmental forms differ in size, infectivity, and division capacity. In addition to these characteristics, both forms also differ in their redox status: EBs are oxidized and RBs are reduced (Fig. 1A). Based on this information, we hypothesized that changing redox potential is a critical factor in the process of differentiation from one form to the other. We named this the “redox threshold hypothesis”. In this scenario, as soon as a given RB has crossed an oxidative threshold, the activity of critical proteins is modified to trigger differentiation to the EB (Fig. 1B). AhpC is an antioxidant enzyme, and several reports have indicated that ablation of *ahpC* creates highly oxidized conditions in bacteria (Feng et al., 2020; Zhang et al., 2019). Therefore, we hypothesize that AhpC, which maintains redox homeostasis in other bacteria, is a critical factor in mediating developmental cycle progression and that altering its activity will impact developmental cycle progression consistent with the redox threshold hypothesis (Fig. 1C).

Overexpression of *ahpC* has minimal impact on chlamydial growth

To study the effect of AhpC on chlamydial developmental cycle progression, we first generated an *ahpC* overexpression (OE) strain using a plasmid encoding an anhydrotetracycline (aTc)-inducible *ahpC* (untagged) and transformed it into a *C. trachomatis* L2 strain lacking its endogenous plasmid (-pL2). The same plasmid vector backbone (i.e., encoding mCherry in place of *ahpC*) was used as an empty vector control (EV). HeLa cells were infected with these transformants, and, at 10 hpi, expression of the construct was induced or not. Lacking an antibody against AhpC, overexpression of *ahpC* was validated by reverse transcription-quantitative PCR (RT-qPCR). Here, an approximate 1-log increase in transcripts of *ahpC* was detected at 14 and 24 hpi in the induced strain in comparison to the uninduced strain (Fig. 2A). Immunofluorescence analysis (IFA) was performed at 24 hpi to examine the organisms’ morphology and overall inclusion growth. For IFA, individual bacteria were labeled with an anti-

139 major outer membrane protein (MOMP) antibody, and DAPI was used to stain for DNA. IFA
140 imaging revealed that there was no observable impact on the morphology of the EV control
141 strain under the conditions tested. In contrast, we did note that overexpression of
142 *ahpC* increased the overall inclusion area (Fig. 2B and 2C). We next quantified the total number
143 of bacteria (i.e., both RBs and EBs) by measuring genomic DNA and observed a significant
144 increase in gDNA levels at 24 hpi in response to increased *ahpC* expression (Fig. 2D). Although
145 inclusions were larger in area and contained more total bacteria as assessed by gDNA levels
146 when overexpressing *ahpC*, recoverable inclusion forming units (IFUs; a proxy for infectious
147 EBs) were significantly lower under these conditions at 24 hpi (Fig. 2E). However, by 48 hpi, the
148 difference between the induced and uninduced conditions, although still reduced, was not
149 statistically significant. The inclusion forming unit analysis only measures viable EBs from a
150 population, suggesting that AhpC overexpression skews the ratio of RBs to EBs. Overall, these
151 data support the hypothesis that overexpressing *ahpC* delays production of infectious EBs.

152 **Overexpression of *ahpC* confers resistance to peroxides in *Chlamydia***

153 AhpC is an important peroxiredoxin involved in oxidative damage defense. Before determining
154 whether increased *ahpC* expression impacts chlamydial sensitivity to oxidizing agents, we first
155 sought to determine the response of *C. trachomatis* to inorganic or organic hydroperoxides such
156 as hydrogen peroxide (H_2O_2), cumene hydroperoxide (CHP), and tert-butyl hydroperoxide
157 (TBHP) as well as peroxynitrite (PN). To do this, we evaluated the sensitivity of HeLa cells,
158 infected or not with the empty vector (EV) control strain, to different concentrations of oxidizing
159 agents using a viability assay. Both uninfected and EV-infected HeLa cells tolerated up to 1 mM
160 oxidizing agents for 30 min (Fig. S1). Next, different concentrations (lower than 1 mM) of these
161 oxidants were tested on wild-type (WT) *C. trachomatis* L2/434/Bu (*Ctr* L2). HeLa cells were
162 infected with *Ctr* L2 and, at 16 hpi, were exposed to different concentrations of exogenous
163 oxidizing agents for 30 min only, before washing out the oxidizing agents and replacing the
164 media. Samples for IFU and IFA assays were then collected at 24 hpi to assess effects of the

165 oxidizing agents on growth of *Ctr* L2. 62.5 μM concentration of all three inorganic and organic
166 peroxides had no appreciable effect on IFUs, and inclusion size and morphology also remained
167 unaffected at this sublethal concentration. The concentrations of inorganic and organic
168 peroxides that resulted in a decrease in IFUs to ~50% of the untreated culture were 500 μM
169 (H_2O_2) and 250 μM (CHP and TBHP), respectively, with a concurrent decrease in inclusion size.
170 1 mM H_2O_2, CHP, and TBHP caused >90% reduction in IFUs and small inclusions. PN at 1 mM
171 concentration was less effective than other oxidizing agents and showed only a ~30% decline in
172 IFUs compared to the untreated culture (Fig. S2).

173 To further examine the antioxidant functions of AhpC, we next exploited our *ahpC*
174 overexpression strain to explore its capability to protect chlamydiae from oxidizing agents. Both
175 *ahpC* OE and EV strains were used to infect HeLa cells and, at 10 hpi, expression of the
176 constructs was induced or not with 1 nM aTc. At 16 hpi, infected cells were exposed to various
177 concentrations of exogenous oxidizing agents for 30 min. At 24 hpi, IFU and IFA samples were
178 collected to measure chlamydial growth and assess chlamydial morphology, respectively. As
179 shown in Figure 3A, 3B, and S3, the *ahpC* overexpression strain showed increased resistance
180 to all oxidants tested as the mean IFUs and the size of inclusions were greater than that of the
181 uninduced but treated control. There was no change in bacterial growth and morphology in the
182 case of 62.5 μM concentrations of oxidizing agents, which was anticipated since we determined
183 this was a sublethal concentration. The resistant phenotype was more evident at the higher
184 concentrations of H_2O_2, CHP, and TBHP. Overexpression of *ahpC* also contributed to higher
185 resistance against PN. Conversely, the empty vector control strain behaved as expected (i.e.,
186 like WT) in the presence of oxidizing agents, with similar results observed in the presence or
187 absence of aTc (Fig. 3C, 3D, and S3). Collectively, these data demonstrate that the chlamydial
188 AhpC possesses antioxidant activity, as expected, and that increased *ahpC* expression is
189 protective for *Chlamydia* in the presence of increased oxidative stress.

Knockdown of *ahpC* negatively impacts chlamydial growth

To further define the function(s) of AhpC in the chlamydial developmental cycle, we used a novel dCas12-based CRISPR interference (CRISPRi) strategy adapted for *Chlamydia* by our lab (Ouellette, 2018; Ouellette et al., 2021). We generated an *ahpC* knockdown strain harboring the pBOMBL12CRia with a crRNA targeting the *ahpC* 5' intergenic region (plasmid designated as pL12CRia(*ahpC*)). We used a strain carrying a pL12CRia plasmid with a crRNA with no homology to any chlamydial sequence (i.e., non-targeting [NT]) to serve as a negative control. To confirm the knockdown of *ahpC*, RT-qPCR was employed. Here, we infected HeLa cells with the *ahpC* knockdown (*ahpC* KD) or NT strains and induced dCas12 expression or not at 10 hpi using 1 nM aTc. Nucleic acid samples were harvested at 14 hpi and 24 hpi. RT-qPCR analysis of the *ahpC* KD revealed approximately 90% reduction of *ahpC* transcripts compared to the uninduced control, thus confirming the knockdown of *ahpC* (Fig. 4A). In the case of the NT control, there was no effect on *ahpC* transcripts. IFA of these strains revealed noticeably smaller inclusions after blocking expression of *ahpC* as compared to the uninduced sample or the NT conditions (Fig. 4B). We next measured total bacterial counts using genomic DNA. Surprisingly, even though inclusions were smaller during *ahpC* knockdown, we observed slightly higher gDNA levels at 14 hpi compared to the uninduced control, followed by only a small increase from 14 to 24 hpi (Fig. 4C). In contrast, the uninduced strain showed a logarithmic increase in gDNA levels during this timeframe. These effects were not detected for the NT strain (Fig. 4C). To further explore the effect of reduced *ahpC* transcripts in *Chlamydia*, IFU assays were performed. IFU analysis exhibited severely reduced progeny (>90%) in *ahpC* knockdown compared to its respective uninduced control at both time points assessed (24 and 48 hpi) (Fig. 4D). In contrast, the NT strain showed less than a 50% reduction after inducing dCas12 expression at these timepoints consistent with prior observations that dCas12 expression slightly delays developmental cycle progression (Hatch & Ouellette, 2023; Reuter et al., 2023).

215 Taken together, these analyses indicate that reducing *ahpC* levels and/or activity severely
216 disrupted chlamydial growth and development.

217 To investigate whether *ahpC* knockdown resulted in increased ROS levels in the bacteria
218 (Zhang et al., 2019), the intracellular ROS levels were measured in infected cells in *ahpC*
219 knockdown conditions and compared to the uninduced control condition and uninfected cells.
220 We used the cell-permeable, fluorogenic dye CellROX Deep Red to measure ROS levels. This
221 dye remains non-fluorescent in a reduced state and exhibits bright fluorescence once oxidized
222 by ROS. ROS generation was measured in uninfected and *ahpC* KD-infected HeLa cells at 24
223 and 48 hpi. As shown in Figure 4E, *ahpC* knockdown resulted in significantly higher ROS than
224 the uninfected or infected but uninduced samples at both 24 hpi and 48 hpi time points. These
225 results together indicate that AhpC plays an important role in counteracting oxidative stress by
226 reducing ROS in *C. trachomatis*.

227 **Knockdown of *ahpC* sensitizes *Chlamydia* to oxidizing agents**

228 As overexpression of *ahpC* resulted in increased resistance to oxidizing agents, we next
229 explored whether knockdown of *ahpC* resulted in increased sensitivity to such agents. As
230 described above, *ahpC* KD and NT strains were used to infect HeLa cells and, at 10 hpi,
231 expression of dCas12 was induced or not with 1 nM aTc. Considering that the *ahpC* KD already
232 demonstrated reduced IFUs and inclusion sizes at 24 hpi, only sublethal concentrations (62.5
233 μM) of exogenous oxidizing agents were applied. At 24 hpi, IFA and IFU analyses were
234 performed to quantify the effect of the oxidants on chlamydial growth in the absence of *ahpC*
235 activity. Under conditions of *ahpC* knockdown, even sublethal concentrations (62.5 μM) of H_2O_2,
236 CHP, or TBHP further reduced the inclusion size, and the IFU data revealed a decrease from
237 >90% to <30% in comparison to the untreated control (Fig. 5A, 5B, and S4). Reduced
238 expression of *ahpC* also affected the survival of *Chlamydia* against peroxynitrite. Notably, there
239 was no significant change in the NT control strain in the uninduced and induced samples in

240 response to oxidizing agents as assessed by IFU and IFA (Fig. 5C, 5D, and S4). These data
241 further support that the chlamydial AhpC is a critical antioxidant enzyme in these bacteria.

242 **Complementation restores the growth and resistance to low levels of peroxide stress of**
243 **the *ahpC* knockdown strain**

244 To validate that the impaired growth, altered inclusion morphology, and enhanced sensitivity to
245 peroxides were due to the decreased level/activity of AhpC, we generated a complemented
246 strain of *ahpC* knockdown. For the construction of the *ahpC* complementing plasmid, the *ahpC*
247 gene was cloned and transcriptionally fused 3' to the dCas12 in the pL12CRia(*ahpC*)
248 knockdown plasmid. Here, the complementing *ahpC* allele is also under the control of the aTc-
249 induced P*tet* promoter and is co-expressed with the aTc-inducible dCas12. Consequently, the
250 *ahpC* knockdown effect is ablated, and the observed phenotypes should be restored. After
251 inducing *dCas12-ahpC* expression with aTc, the resultant strain was verified by RT-qPCR.
252 Increased transcripts for *ahpC* were quantified under these conditions, indicating successful
253 complementation of the knockdown effect (Fig. 6A). Of note, the *ahpC* transcript levels
254 remained elevated in comparison to the uninduced control at the 24hpi time point. After
255 confirming this strain, we measured genomic DNA to quantify total bacteria and performed IFA
256 and IFU assays to examine if complementation restored the phenotypes observed during *ahpC*
257 knockdown. These assays revealed normal inclusion morphology, gDNA levels, and EB progeny
258 production in the complemented strain, indicating successful complementation of the
259 knockdown phenotype (Fig. 6B, C, and D). Of note, a C-terminal 6xHis tagged AhpC was not
260 capable of complementing the knockdown phenotype (data not shown), indicating a requirement
261 for a free C-terminus in the function of AhpC in *Chlamydia*. Previous studies in other bacteria
262 have revealed that the C-terminal residues in AhpC play a crucial role in the structural stability
263 and enzymatic activity of AhpC (Dip et al., 2014; Feng et al., 2020; Wan et al., 2021).

264 We next assessed whether complementation of the knockdown phenotype could also
265 restore the resistance to low levels of peroxide stress. As in previous experiments, a sublethal

concentration of oxidizing agents was added for 30' at 16 hpi after having induced *dCas12-ahpC* expression at 10 hpi. Consistent with the growth parameters (Fig. 6B-D), the complemented strain showed wild-type responses in these conditions (Fig. 6E, 6F, and S4). These data indicate that the enhanced susceptibility of the *ahpC* knockdown strain to oxidizing agents was due to the reduced levels of *ahpC* and not an indirect effect of knockdown.

We predicted that the growth defects resulting from higher production of ROS during *ahpC* knockdown could be rescued by treating the *ahpC* KD with ROS scavengers. To test this prediction, we utilized two characterized ROS scavengers, DMTU (*N,N'-dimethylthiourea*) and α-tocopherol, which scavenge H_2O_2 and peroxyl radical, respectively (Hollander-Czytko et al., 2005; Kiffin et al., 2006; Walch et al., 2015). First, the effect of ROS scavengers on uninfected and infected HeLa cells was investigated using a viability assay. This assay revealed that 10 mM DMTU and 100 µM α-tocopherol had no adverse effects on uninfected or EV-infected HeLa cells (data not shown). These same concentrations were tested on WT *Ctr* L2 infected HeLa cells in untreated and 500 µM H_2O_2 treated conditions to test the potency of these scavengers to rescue growth defects associated with this concentration of oxidizing agent. Scavengers were added at 9.5 hpi and washed away at 16 hpi - the time of addition of H_2O_2 in the respective samples. At 16.5 hpi, after 3 wash steps, scavengers were added again with fresh media, and, at 24 hpi, bacterial growth and morphology were assessed using IFU and IFA assays. Neither scavenger had a significant impact on chlamydial morphology or infectious progeny. In the case of peroxide (500 µM H_2O_2) treated samples, scavengers restored IFUs from ~50% to ~100%, and inclusion size was also recovered (Fig. S5A and B).

Next, the effect of the ROS scavengers under *ahpC* knockdown conditions was assessed. In this experiment, scavengers were added at 9.5 hpi to provide the protective effect of scavengers before reducing the activity of *ahpC*. At 10 hpi, knockdown was induced or not with 1 nM aTc, and, at 14 hpi, scavengers were added again. At 24 hpi, IFU and IFA samples

were collected to examine bacterial growth and morphology to assess the effect of ROS scavenging on the *ahpC* knockdown phenotype. As shown in Fig. 6G and 6H, both ROS scavengers had a positive impact on restoring growth of the *ahpC* knockdown strain; inclusions were larger, and IFUs were increased from <10% to >90% in the presence of scavengers in the induced samples. These data provide compelling evidence that the adverse effects of *ahpC* knockdown are due to increased ROS accumulation in this strain.

Chlamydial developmental cycle progression is altered by *ahpC* knockdown/ overexpression

Whereas the overexpression of AhpC delayed overall developmental progression and was consistent with our hypothesis, the results with the *ahpC* knockdown strain appeared to refute our hypothesis given the apparent decrease in IFUs and smaller inclusion sizes after knockdown. To investigate the effects of changes in redox potential on chlamydial developmental cycle progression, we performed a transcriptional analysis of well-characterized late-cycle genes associated with secondary differentiation (*hctA*, *hctB*, *glgA*, *tsp,* and *omcB*) (Belland et al., 2003; Gehre et al., 2016; Newhall, 1987; Ouellette et al., 2006; Swoboda et al., 2023). In the uninduced samples, transcript levels of all the tested late genes were higher at 24 hpi compared to 14 hpi, indicating their normal expression during the late stage of the developmental cycle. In comparison to the uninduced control, under conditions of *ahpC* knockdown, significantly higher expression of *hctA*, *hctB*, *omcB, tsp,* and *glgA* was observed at the mid-developmental cycle timepoint of 14 hpi (Fig. 7A). At 24 hpi, expression of these genes was comparable between the uninduced and induced conditions in the *ahpC* knockdown strain. In contrast, the complementation strain showed no increase in the expression of these tested late genes at 14 hpi, and *tsp* and *glgA* transcripts were reduced (Fig. 7C). Consistent with our model, the overexpression of *ahpC* resulted in significantly lower expression of *hctA*, *hctB*, *omcB, tsp*, and *glgA* at 14 and 24 hpi (Fig. 7D), suggesting a delayed transition to EBs.

316 Given the increase in late gene expression during *ahpC* knockdown at an earlier time
317 point in the developmental cycle than normal, we reasoned that the increase in oxidizing
318 conditions might prematurely trigger secondary differentiation and EB production. However,
319 complicating such an analysis is that fewer RBs are present to convert to EBs, which would
320 result in overall lower IFU yields as we had measured at 24 and 48 hpi (Fig. 4D). Nonetheless,
321 to assess EB production more rigorously at earlier time points in the developmental cycle, we
322 performed a growth curve analysis to precisely measure IFUs at two-hour intervals from 16 to
323 24 hpi. HeLa cells were infected, and knockdown was induced or not at 10 hpi with 1 nM aTc. At
324 the indicated time points, IFU samples were collected and quantified. Consistent with our
325 prediction, this experiment revealed higher IFUs (i.e., EBs) at 16 and 18 hpi during *ahpC*
326 knockdown compared to the uninduced samples (Fig. 7B). This difference was statistically
327 significant at 18 hpi. However, further EB production was stalled, with the uninduced strain
328 continuing to produce EBs such that, by 24 hpi, there were significantly higher EB yields under
329 these conditions (as noted in Fig. 4D). These data show that the phenotypic consequence of
330 higher expression at 14 hpi of genes functionally related to EBs is the concomitant earlier
331 production of EBs. These data underscore that reduced activity of *ahpC* causes earlier
332 secondary differentiation in *C. trachomatis*.

333 ***ahpC* knockdown activates transcription of late-cycle genes when bacterial replication is**
334 **blocked**

335 We detected earlier expression of EB-related genes during *ahpC* knockdown and were curious
336 if the *ahpC* knockdown condition could activate these genes under conditions when the
337 chlamydial developmental cycle is blocked. Pathogenic *Chlamydia* species undergo a polarized
338 cell division process, in which peptidoglycan is transiently synthesized only at the division
339 septum (Abdelrahman et al., 2016; Cox et al., 2020; Ouellette et al., 2020). As a result, during
340 penicillin treatment, division of RBs is blocked (Moulder, 1993; Moulder et al., 1956; Ouellette et
341 al., 2020). However, the bacteria continue to grow in size resulting in aberrantly enlarged RBs

342 (Barbour et al., 1982; Matsumoto & Manire, 1970; Ouellette et al., 2012), in which EB-related
343 genes are not transcribed and production of EBs is inhibited (Ouellette et al., 2006; Panzetta et
344 al., 2018).

345 To examine this, we generated an *ahpC* KD strain with spectinomycin resistance (*ahpC*
346 KD-spec) and validated its phenotype as being the same as the penicillin-resistant *ahpC* KD
347 strain. This new strain, *ahpC* KD-spec, was used to infect HeLa cells, and knockdown was
348 induced or not at 10 hpi with 1 nM aTc. At the same time, samples were treated or not with 1
349 unit per mL of penicillin (Pen). RNA samples were harvested at 16 and 24 hpi and processed for
350 RT-qPCR (Fig. S6B-D). IFA controls from these different conditions demonstrated the expected
351 phenotypes (Fig. S6A). For example, Pen treatment caused aberrantly enlarged RBs,
352 irrespective of *ahpC* KD, whereas *ahpC* KD itself caused smaller inclusions. Similarly, *ahpC* KD
353 resulted in reduced *ahpC* transcripts in the induced conditions irrespective of the presence of
354 Pen (Fig. S6B). We next quantified transcript levels for the late genes *hctA* and *hctB* in these
355 different conditions (Fig. S6C and D). As expected, in the uninduced and untreated condition,
356 both transcripts had higher expression at 24 hpi, indicating their regular developmental
357 expression during the late stage of the developmental cycle. Consistent with prior observations
358 (Ouellette et al., 2006), transcript levels of these genes in uninduced+Pen conditions was low.
359 As we previously noted (Fig. 7A), the transcripts of *hctA* and *hctB* are higher in the induced than
360 uninduced samples at 16 hpi in the absence of Pen. Interestingly, in the induced+ Pen condition,
361 these genes had higher expression at 24 hpi than the uninduced+Pen control. At 16 hpi, their
362 expression was either higher or similar between both samples (i.e., induced+Pen and
363 uninduced+Pen). Collectively, these data support our observation that *ahpC* knockdown
364 activates the transcription of late-cycle genes – even under conditions where developmental
365 cycle progression is blocked.
366

DISCUSSION

Secondary differentiation (differentiation from RBs to EBs) is an essential step for chlamydial growth and survival, but there is a dearth of information regarding the mechanisms of its regulation. EBs and RBs have significantly different proteomic repertoires, and our group has identified critical functions for the cytoplasmic ClpXP and ClpCP and periplasmic Tsp proteases during secondary differentiation (Pan, Jensen et al., 2023; Swoboda et al., 2023; Wood et al., 2022). The *tsp* gene, in addition to another late-cycle gene, *hctB*, is transcriptionally regulated by sigma factor 28 (σ^{28}) (Hatch & Ouellette, 2023). Another sigma factor, σ^{54} has been linked to regulation of outer membrane components, type III secretion system components, and other genes typically expressed late in development (Hatch & Ouellette, 2023; Soules, LaBrie, et al., 2020) . In addition to the two minor sigma factors, σ^{28} and σ^{54}, *Chlamydia* encodes one major sigma factor, σ^{66}, which is transcriptionally regulated by the relative levels of RsbV1 (antagonist) and RsbW (anti-sigma factor) (Thompson et al., 2015). This Rsb system senses ATP availability and has been proposed to regulate σ^{66} (Thompson et al., 2015). A related study from Soules et al. (Soules, Dmitriev, et al., 2020) showed that TCA intermediates act as ligands for RsbU, thereby linking the Rsb system to the TCA cycle and ATP synthesis. Collectively, these data show that post-translational mechanisms drive secondary differentiation in *Chlamydia*. However, no definitive “switch” that triggers this step has been identified.

Aside from the clear morphological and functional differences between the EB and RB, they also differ in their redox status: EBs are more oxidized whereas RBs are more reduced (Wang et al., 2014). This same study noted that the overall redox status of the host cell was relatively unchanged throughout the developmental cycle, suggesting that changes in the bacteria were driven by endogenous processes (i.e., metabolism). Though *Chlamydia* is dependent on its host for most of its energy requirements, it has some metabolic activities, such as a partial TCA cycle and oxidative phosphorylation (Gerard et al., 2002; Iliffe-Lee & McClarty, 1999) that can be possible sources of intracellular ROS. We hypothesize that accumulating

redox stress from its metabolic activities serves as a signal to trigger secondary differentiation from RBs to EBs. There is a paucity of knowledge on how *C. trachomatis* modulates oxidative stress during disease pathogenesis. However, some studies explored the effects of redox changes on *Chlamydia* growth. Boncompain et al. reported that infection of *C. trachomatis* induced the transient production of ROS by the host cell at a moderate level for the initial few hours of infection only (Boncompain et al., 2010). Another study also found a similar observation about ROS during infection, reporting that *Chlamydia* requires host-derived ROS for its growth (Abdul-Sater et al., 2010). Given that no studies have examined the role of chlamydial proteins related to redox and how these proteins impact the growth of the pathogen, we initiated experiments to investigate the function of a key antioxidant enzyme, AhpC, as a means of testing our hypothesis.

Reactive oxygen species (ROS) generation is an inevitable condition for pathogens growing in aerobic conditions, and resistance against oxidative stress (imbalanced level of ROS) is a key survival mechanism (Fang, 2011). Hence, pathogens have evolved detoxifying proteins, such as peroxiredoxins, to eliminate ROS (Dip et al., 2014; Wang et al., 2004; Yang et al., 2002). AhpC is a 2-cys peroxiredoxin and has been reported to have a crucial role in bacterial physiology, survival, and virulence by scavenging ROS and RNI (Cosgrove et al., 2007; Kimura et al., 2012; Loprasert et al., 2003; Oh & Jeon, 2014). In the process of detoxification of peroxides and peroxynitrite, AhpC is converted into an oxidized dimer, requiring alkyl hydroperoxide reductase AhpF or AhpD to regenerate its activity (Koshkin et al., 2004; Poole & Ellis, 1996; Wong et al., 2017). *C. trachomatis* encodes AhpC (Ct603) but lacks any annotated homologs of AhpF or AhpD. Therefore, it remains an open question how AhpC activity is regulated. Some studies have mentioned *ahpC* as an iron-responsive gene in *Chlamydia* (Brinkworth et al., 2018; Pokorzynski et al., 2019), but there is no detailed investigation to date about the role of this crucial antioxidant in the growth and development of *Chlamydia.*

Using a broad set of methodologies, we created and characterized overexpression and knockdown conditions of *ahpC*. Higher expression of *ahpC* resulted in lower EB production at 24 hpi coupled with a higher number of RBs and larger inclusion size (Fig. 2), suggesting differentiation from RBs to EBs is delayed. The number of EBs is further decreased at 48 hpi, but the difference is not statistically significant. This may be due to the highly oxidized conditions in *Chlamydia* at 48 hpi (Wang et al., 2014) or the inability of *ahpC* overexpression to generate sufficient reducing conditions to neutralize it completely. In our studies, *ahpC* expression was induced at 10hpi, and adequate enzyme levels may not have been sustained later during the developmental cycle. Consistent with studies in other bacteria (Sherman et al., 1999; Zuo et al., 2014), overexpression of *ahpC* created resistance to different oxidants (Fig. 3 and S3), indicating that AhpC is the principal defense mechanism against oxidative stress in *Chlamydia*. During *ahpC* knockdown, the attenuated activity of AhpC severely affected the growth of bacteria (Fig. 4). Notably, the morphology of inclusions during *ahpC* knockdown is strikingly similar to *Chlamydia* treated with a high concentration (1 mM) of oxidizing agents (Fig. 4 and Fig S2), indicating similar scenarios in both conditions. This was further supported by the increased sensitivity of *ahpC* knockdown to sublethal concentrations of oxidants (Fig. 5 and S4). Again, this observation is consistent with previous data from other bacteria (Cosgrove et al., 2007; Seaver & Imlay, 2001; Storz et al., 1989; Zhang et al., 2019).

An essential aspect of the scavenging activity of AhpC for many bacterial pathogens in which it has been studied is that it works best with endogenous (i.e., low) levels of H_2O_2. These bacteria, such as *Staphylococcus aureus* and *Yersinia pseudotuberculosis*, encode catalases, which have high Km for hydrogen peroxide and serve a predominant role in scavenging exogenous H_2O_2 (Cosgrove et al., 2007; Wan et al., 2021). Catalases can detoxify H_2O_2 at high levels (millimolar levels) and are crucial in responding to external H_2O_2 stress (Mishra & Imlay, 2012). The *ahpC* mutants in these bacteria became sensitive to organic peroxides but resistant to H_2O_2 due to higher catalase activity as a compensatory response to the lack of AhpC

(Antelmann et al., 1996; Mongkolsuk et al., 2000; Ochsner et al., 2000). Further, simultaneous mutations in both catalase and *ahpC* displayed drastically enhanced sensitivity to all oxidizing agents tested (Cosgrove et al., 2007; Ezraty et al., 2017; Seaver & Imlay, 2001). *C. trachomatis* does not encode a catalase gene (Boncompain et al., 2014; Rusconi & Greub, 2013), and hypersensitivity of *ahpC* knockdown to both inorganic and organic peroxides indicates the absence of catalase and establishes that AhpC is the primary scavenger of ROS in *C. trachomatis*. We did not observe significant effects of PN with AhpC expression. One possible explanation may be our study's concentration (1 mM) of PN. Higher concentrations of PN could not be used due to toxic effects on the host cell. The other possibility may be the presence of some other unknown mechanism(s) to detoxify PN. For example, *Chlamydia* also encodes a superoxide dismutase (SOD) that may prevent the accumulation of the necessary precursors that are needed for PN production. We are currently investigating the function of the chlamydial SOD enzyme.

Previous studies in other bacterial systems indicated that ROS production significantly increased after the deletion of *ahpC* (Zhang et al., 2019). Similarly, in *Chlamydia* during *ahpC* knockdown, the ROS level was dramatically higher. Its ability to dissipate ROS produced by exogenous oxidative stress was severely compromised (Fig. 4E). Further, the addition of ROS scavengers to the culture medium rescued the negative phenotypes associated with *ahpC* knockdown (Fig. 6G and H). This strongly suggests that, in the absence of AhpC, higher amounts of reactive oxygen species accumulate in *Chlamydia* and that the negative impact on growth during *ahpC* knockdown is due to highly oxidized conditions in the organism. Moreover, for the complete restoration of inclusion size, multiple doses of scavengers were required throughout the experiment, further emphasizing that the internal chlamydial environment is oxidized and/or susceptible to oxidation in the absence of AhpC. These findings suggest that AhpC in *Chlamydia* is indispensable, having a functional role even more extensive than previously reported in other bacteria.

Interestingly, in our RT-qPCR study, late-cycle genes such as *hctA*, *hctB*, *glgA, omcB*, and *tsp* are expressed at a higher level at an earlier time (14 hpi) in the chlamydial developmental cycle as a result of reduced AhpC activity (Fig. 7). Notably, in the developmental cycle of *C*. *trachomatis*, only RBs are present at 14 hpi, and secondary differentiation starts after 16 hpi (Abdelrahman & Belland, 2005). Expression of most of the late-cycle genes occurs after this time in the developmental cycle (Belland et al., 2003). Among the tested late-cycle genes, *hctA* and *hctB* encode histone-like proteins responsible for chromosomal condensation during the differentiation of RBs into EBs. The *hctA* gene is among the first to be transcribed in the late-stage (Chiarelli et al., 2020). The other three late genes, *tsp*, *omcB*, and *glgA*, are all well-characterized late genes associated with secondary differentiation. Tsp is a periplasmic protease thought to be crucial in the degradation of RB-specific periplasmic proteins during secondary differentiation in *C. trachomatis* (Swoboda et al., 2023). OmcB is responsible for the rigid cell wall and osmotic stability of the EBs (Mygind et al., 1998; Newhall, 1987). GlgA is a non-essential secretory protein involved in glycogen metabolism and is responsible for glycogen accumulation in the inclusion lumen at late stages of the developmental cycle (Gehre et al., 2016; Sun et al., 2020). One crucial point to consider is the redox status of *Chlamydia*. 14 hpi is when reduced RBs predominate with virtually no oxidized EBs detectable. However, we established that *ahpC* knockdown shifts the redox status of the bacteria towards oxidation. Hence, the earlier and significantly higher detection of transcripts for these late-cycle genes indicate earlier secondary differentiation in the *ahpC* knockdown. Importantly, *ahpC* complementation during knockdown restored the regular developmental expression of these late-cycle genes, further supporting this phenotype was due to the highly oxidized conditions created by reduced AhpC activity.

The higher expression of genes functionally related to EBs and EB production at an early stage of the chlamydial developmental cycle indicates earlier secondary differentiation as an outcome of diminished activity of *ahpC* in *C. trachomatis*. Consequently, increased late gene

transcription should have the phenotypic effect of causing earlier production of EBs. Indeed, we quantified more IFUs (proxy for EBs) in the *ahpC* knockdown at 16 and 18 hpi compared to the uninduced control condition. In contrast, for the AhpC overexpression strain, the expression of these late-cycle genes in the induced conditions compared to the uninduced control at 24 hpi is significantly lower, indicating reduced production of EBs. These data support our hypothesis that the developmental cycle is delayed in the reduced environment. We propose a simple model to explain these scenarios (Fig. 8). During *ahpC* KD, higher amounts of ROS accumulation in the bacterium create highly oxidized conditions. As secondary differentiation is asynchronous and RBs divide through an asymmetric budding mechanism (Ouellette et al., 2020), ROS levels are unevenly distributed between mother and daughter cell. This difference will lead some RBs to breach an oxidative threshold sooner, allowing activation of late genes and secondary differentiation earlier than other RBs. In contrast, *ahpC* overexpression scavenges ROS at a greater level leading to a more reducing environment. This results in a delay in achieving the oxidative threshold, thus allowing RBs to continue to divide before committing to secondary differentiation. Taken together, our data directly link oxidation state and secondary differentiation in *Chlamydia*. Ongoing studies are focused on characterizing redox-sensitive chlamydial proteins to understand which specific factors drive the shift from RBs to EBs (or EBs to RBs) in *C. trachomatis*.

MATERIALS AND METHODS

Strains and cell culture

For chlamydial transformation, McCoy mouse fibroblast cells (kind gift of Dr. Harlan Caldwell (NIH/NIAID)) were used. Human cervix adenocarcinoma epithelial HeLa cells (kind gift of Dr. Harlan Caldwell (NIH/NIAID)) were used for RT-qPCR, immunofluorescence assays (IFA), inclusion forming unit assays (IFU), viability assays, oxidative stress, ROS measurements, and ROS scavenger assays. Both cell types were routinely grown and passaged in Dulbecco's modified Eagle's medium (DMEM; Gibco, Waltham, MA) supplemented with 10% fetal bovine serum (FBS; Sigma, St. Louis, MO) and 10 µg/mL gentamicin (Gibco, Waltham, MA) at 37^0C and 5% CO2. All strains were verified to be Mycoplasma-negative using LookOut mycoplasma PCR detection kit (Sigma). For chlamydial transformations, *Chlamydia trachomatis* serovar L2 EBs lacking the endogenous pL2 plasmid (kind gift of Dr. Ian Clarke, University of Southampton) were used (Wang et al., 2011). Wild-type, density gradient-purified *Chlamydia trachomatis* 434/Bu (ATCC VR902B) EBs were used for sensitivity to oxidizing agents and ROS scavenger assays. Molecular biology reagents, oxidizing agents, scavengers, and CellROX Deep Red dye were purchased from Thermo Fisher unless otherwise noted.

Plasmid construction

The primers, gBlock gene fragments, plasmids, and bacterial strains used for molecular cloning are listed in Table S1 in the supplemental material. Constructs for chlamydial transformation were cloned using high-fidelity (HiFi) cloning system from New England BioLabs (NEB). Primers were designed using the NEBuilder online primer generation tool (https://nebuilderv1.neb.com). For the overexpression strain, the *ahpC* gene was amplified by PCR with Phusion DNA polymerase (NEB) using *C. trachomatis* serovar L2 434/Bu genomic DNA as a template. The PCR product was purified using a PCR purification kit (Qiagen, Hilden, Germany). The HiFi assembly reaction was performed as per the manufacturer's instructions in conjunction with the pBOMBDC plasmid digested with Fast Digest EagI and KpnI enzymes and dephosphorylated

with FastAP (Thermo Fisher, Waltham, MA). The HiFi reaction mix was transformed into *E. coli* 10β (NEB). Plasmids were first confirmed by restriction enzyme digestion, and final verification of insert was performed using Sanger sequencing. A dCas12-based CRISPRi approach was used for *ahpC* knockdown generation (Ouellette et al., 2021). The pBOMBL12CRia plasmid having anhydrotetracycline (aTc) inducible catalytically dead dCas12 protein was used as vector. A crRNA targeting the 5' intergenic region of *ahpC* was designed and ordered as a presynthesized DNA fragment. For *ahpC* knockdown construct, 2 ng of the gBlock (Integrated DNA Technologies [IDT], Coralville, IA) listed in Table S1 was combined with 25 ng of BamHI-digested, alkaline phosphatase-treated pBOMBL12CRia(e.v.)::L2 in a HiFi reaction according to the manufacturer's instructions (NEB). The plasmid was transformed into NEB 10β cells and verified by Sanger sequencing prior to transformation into *Chlamydia trachomatis*. To generate the complementation strain, the *ahpC* gene was amplified using primers listed in Table S1 and fused with the *ahpC* knockdown construct (i.e., pBOMBL12CRia (*ahpC*)) digested with the Fast Digest restriction enzyme SalI (Thermo Fisher) and alkaline phosphatase-treated, using the HiFi reaction as mentioned above.

Chlamydial transformation

Chlamydial transformations were performed using a protocol described previously, with some modifications (Mueller et al., 2017). One day before transformation, 1 x 10^6 McCoy cells were seeded in one 6-well plate, and two wells were used per plasmid transformation. Briefly, for each well of the 6-well plate, 2 µg of sequenced verified plasmids were incubated with 2.5 x 10^6 *C. trachomatis* serovar L2 without plasmid (-pL2) EBs in 50 µL Tris-$CaCl_2$ (10 mM Tris, 50 mM CaCl2, pH 7.4) at room temperature for 30 min. McCoy cells were washed with 2 mL Hank's Balanced Salt Solution (HBSS; Gibco), and 1 mL HBSS was added back into each well. 1 mL of HBSS was added to each transformant mixture, and one well of a 6-well plate was infected using this transformation solution. Cells were centrifuged at 400 × g for 15 min at room temperature followed by 15 min incubation at 37°C. HBSS was aspirated and replaced with

antibiotic-free DMEM. At 8 hpi, 1 μg/mL of cycloheximide and 1 or 2 U/mL of penicillin G or 500 μg/mL spectinomycin were added to the culture media. The infection was passaged every 48 h until a population of penicillin or spectinomycin resistant, green fluorescent protein (GFP) positive *C. trachomatis* was established. The chlamydial transformants were then serially diluted to isolate clonal populations. These isolated populations were further expanded and frozen at -80^{0}C in a sucrose phosphate solution (2SP). To verify plasmid sequences, DNA was harvested from infected cultures using the DNeasy kit (Qiagen) and transformed into NEB 10β for plasmid propagation. Isolated plasmids were then verified by restriction digest and Sanger sequencing.

Inclusion forming unit assay

Inclusion forming unit assay was performed to determine the infectious progeny (number of EBs) from a primary infection based on inclusions formed in a secondary infection. *C. trachomatis* transformants were infected into HeLa cells and induced or not with 1 nM aTc at 10 hpi. At 24 and 48 hpi, samples were harvested by scraping three wells of a 24-well plate in 2 sucrose-phosphate (2SP) solution and lysed via a single freeze-thaw cycle, serially diluted, and used to infect a fresh HeLa cell monolayer and allowed to grow for 24 h. Samples were fixed with methanol, stained with a goat antibody specific to *C. trachomatis* major outer membrane protein (MOMP; Meridian Biosciences, Memphis TN) followed by staining with donkey antigoat Alexa Fluor 594-conjugated secondary antibody (Invitrogen) and titers were enumerated using a 20x lens objective. All experiments were performed three times for three biological replicates. Induced values were expressed as a percentage of the uninduced values, which was considered as 100%.

Immunofluorescence assay

HeLa cells were cultured on glass coverslips in 24-well tissue cultures plates at 2 x 10^5 cells/well, infected with the relevant strains, and, at 10 hpi, samples were induced or not with 1 nM aTc. At 24 hpi, samples were fixed and permeabilized using 100% methanol. Organisms

were stained with anti-MOMP (Meridian Biosciences) primary antibody for all the strains and primary mouse anti-Cpf1 (dCas12) (Sigma-Millipore) for knockdown or complementation samples. Donkey anti-goat Alexa Fluor 594-conjugated secondary antibody (Invitrogen) was used to visualize *Chlamydia* in all the samples, and donkey anti-mouse Alexa Fluor 488-conjugated secondary antibody (Invitrogen) was used for dCas12 expression. DAPI (Invitrogen) was used for visualization of host and bacterial cell DNA. These stained coverslips were mounted on glass slides using ProLong glass antifade mounting media (Invitrogen) and imaged using a 100x lens objective on a Zeiss Axioimager Z.2 equipped with Apotome.2 optical sectioning hardware and X-Cite Series 120PC illumination lamp using a 2MP Axiocam 506 monochrome camera.

Nucleic acid extraction and RT-qPCR

HeLa cells were seeded in 6-well tissue culture plates, infected with the *C. trachomatis* transformants, and induced or not at 10 hpi with 1 nM aTc. For each condition, triplicate wells were used for simultaneous harvest of RNA (for transcript analysis by RT-qPCR), gDNA (to normalize RT-qPCR data and quantification of gDNA), and IFA (to verify the morphological changes in samples in the tested conditions). For RNA extraction, cells were rinsed with DPBS twice and lysed with 1 mL TRIzol (Invitrogen/Thermo Fisher) per well as per manufacturer's instructions. 200 µL of chloroform was added to extract the aqueous layer containing total RNA, which was precipitated with isopropanol. A total of 10 µg of purified RNA was treated with TURBO DNase (Invitrogen/Thermo Fisher) according to the manufacturer's instructions to remove DNA contamination. DNA-free RNA was used for cDNA synthesis using random nonamers (N9; NEB) and SuperScript III reverse transcriptase (Invitrogen/Thermo Fisher) following the manufacturer's instructions. cDNA samples were diluted 10-fold with molecular biology-grade water and stored at -80°C. A total of 2.5 µL of each diluted cDNA sample was used per well of a 96-well qPCR plate. For each of three biological replicates, each sample was

analyzed in triplicate on a QuantStudio 3 system (Applied Biosystems/Thermo Fisher) using the standard amplification cycle with melting curve analysis. For gDNA, one well of a 6-well plate per condition was scraped in 500 µL DPBS, split in half (i.e., 250 µL), and frozen at -80°C. Each sample was then thawed and frozen twice more for a total of three freeze/thaw cycles, and gDNA was extracted using the DNeasy DNA extraction kit (Qiagen) according to the manufacturer's guidelines. The isolated gDNA was quantified and diluted down to 5 ng/mL prior to use in quantitative PCR (qPCR). A total of 2.5 µL of each diluted gDNA sample was mixed with 10 µL of PowerUp SYBR green master mix in a 96-well qPCR plate and was analyzed on a QuantStudio 3 system (Applied Biosystems). Each sample from each biological replicate was tested in triplicate. For each primer set used, a standard curve of gDNA was generated against purified *C. trachomatis* L2 genomic DNA, and the cDNA levels were normalized to gDNA levels or 16S rRNA for analysis. All experiments were performed three times for three biological replicates. At the same time, morphological differences were monitored in the IFA control, with samples fixed with methanol at the time of harvesting of RNA/gDNA. Staining and imaging were performed as described above.

Viability assay

Cell viability assays were performed using PrestoBlue (Invitrogen/Thermo Fisher). HeLa cells were seeded in 96 well plates and were infected or not with the indicated chlamydial strains (e.g., pBOMBDC.ev). Samples were treated or not as per the experimental parameters (e.g., different concentrations of oxidizing agents or scavengers). Medium without cells was used as the blank control. At the end point, 10% PrestoBlue (v/v) was added in the wells and incubated at 37^0 C for 30 min while protecting the plate from light. Fluorescence was read at excitation 560 nm and emission 590 nm using an Infinite M200 Pro (Tecan). The treated values were expressed as a percentage of the untreated values, which was considered as 100%. All experiments were performed three times for three biological replicates.

Oxidizing agents' susceptibility testing

Susceptibility of host cells and chlamydiae to different oxidizing agents was tested in HeLa cells infected with density gradient-purified *Chlamydia trachomatis* 434/Bu EBs or *C. trachomatis* transformants. For *C. trachomatis* transformants, expression of the construct was induced or not with 1 nM aTc at 10 hpi. At 16 hpi, different concentrations of oxidizing agents were added, and samples were incubated at 37^0C for 30 min. These samples were washed three times with HBSS, fresh DMEM media was added in the wells, and cultures were allowed to grow until 24 hpi. At 24 hpi, inclusion forming unit assays and immunofluorescence analysis were performed as described above.

ROS scavenging by chemical compounds

The scavenging capacity of different ROS scavengers was tested using HeLa cells infected with *Chlamydia trachomatis* 434/Bu EBs or the *ahpC* KD strain. To examine the protective effect of scavengers in the absence or presence of oxidative stress, *Chlamydia trachomatis* 434/Bu EBs infected HeLa cells were used. In these samples, scavengers were added or not at 10 hpi in respective wells. At 16 hpi, wells were washed three times with HBSS, and fresh DMEM containing 500 μM H_2O_2 or not was added. After 30 min, wells were washed three times with HBSS and fresh DMEM containing scavengers or not was added back in the respective wells, which were incubated until 24 hpi prior to collecting samples for IFU assay and IFA analysis. The effect of these scavengers was further tested in *ahpC* KD. HeLa cells were infected with *ahpC* KD, scavengers were added or not at 9.5 hpi before induction at 10 hpi with 1nM aTc. At 14 hpi, scavengers were added again in the respective wells, and, at 24 hpi, samples were collected for IFU assay and IFA.

ROS detection by CellROX Deep Red

Intracellular ROS levels were measured in uninfected and *ahpC* KD-infected HeLa cells using CellROX Deep Red dye (Invitrogen/Thermo Fisher). Samples were induced or not at 10 hpi with 1 nM aTc. Medium without cells was used as the blank control. At 16 hpi, samples were treated or not with 62.5 μM or 1 mM TBHP for 30 min. At the end point, media was removed, samples

were washed three times with DPBS and incubated with CellROX Deep Red dye for 30 min in the dark at 37^0C. Fluorescence was read at excitation 644 nm and emission 665 nm using an Infinite M200 Pro (Tecan). All experiments were performed three times for three biological replicates.

ACKNOWLEDGMENTS

We thank Dr. H. Caldwell (NIH/NIAID) for providing eukaryotic cell lines and Dr. I. Clarke (University of Southampton) for providing the plasmid less strain of *C. trachomatis* serovar L2. We thank Dr. Elizabeth A. Rucks for critical feedback. We thank the members of the Rucks/Ouellette research group for thoughtful discussion of the material presented. Funding for this work was provided by the National Institutes of Health (NIH/NIAID) grants R01AI170688 and R21AI178150 to SPO.

696

697

698

699

700

701

702 **Figure legends:**

703 **Fig. 1** Alterations in redox status of key proteins regulate and drive chlamydial differentiation.
704 (A) Key characteristics of chlamydial developmental forms. (B) Hypothetical model for triggering
705 secondary differentiation through oxidative stress (black angled line). Increasing oxidation of
706 critical protein(s) may lead to earlier differentiation whereas maintaining a reducing environment
707 may delay differentiation. (C) Schematic representation of experimental model for triggering
708 secondary differentiation through altered activity of AhpC. *ahpC* knockdown may lead to earlier
709 differentiation while overexpression of *ahpC* may delay differentiation.

710 **Fig. 2** Overexpression of *ahpC* affects chlamydial growth and differentiation. (A) Transcriptional
711 analysis of *ahpC* in *ahpC* overexpression (*ahpC*) and empty vector (EV) control using RT-qPCR
712 following induction at 10 hpi with 1 nM aTc. RNA and genomic DNA (gDNA) were harvested at
713 14 and 24 hpi and processed as mentioned in materials and methods. Data are presented as a
714 ratio of cDNA to gDNA plotted on a log scale. ***$p < 0.0001$ vs uninduced sample by using two-
715 way ANOVA. Data represent three biological replicates. (B) Immunofluorescence assay (IFA) of
716 *ahpC* and EV at 24 hpi. Construct expression was induced or not at 10 hpi with 1 nM aTc, and
717 samples were fixed with methanol at 24 hpi then stained for major outer membrane protein
718 (MOMP - red) and DAPI (blue) to label DNA. Scale bars = 2 μm. Images were captured using a
719 Zeiss Axio Imager Z.2 with Apotome2 at 100x magnification. Representative images of three
720 biological replicates are shown. (C) Impact of *ahpC* overexpression on inclusion area. Inclusion
721 area of *ahpC* overexpression and EV strains was measured using ImageJ. Experimental

722 conditions were the same as mentioned in section (B). The area of 50 inclusions was measured
723 per condition for each sample. ***p< 0.001 vs uninduced sample by using ordinary one-way
724 ANOVA. Data were collected from three biological replicates. (D) IFU assay of *ahpC*
725 overexpression and empty vector control. Expression of the construct was induced or not at 10
726 hpi, and samples were harvested at 24 or 48 hpi for reinfection and enumeration. IFUs were
727 calculated as the percentage of uninduced samples. **p< 0.001 vs uninduced sample by using
728 multiple paired t test. Data represent three biological replicates. (E) Quantification of genomic
729 DNA (gDNA) determined by qPCR in *ahpC* overexpression and empty vector control. Construct
730 expression was induced or not at 10 hpi with 1 nM aTc, gDNA was harvested at 14 and 24 hpi,
731 and ng gDNA were plotted on a log scale. ***p< 0.0001 vs uninduced sample by using two-way
732 ANOVA. Data represent three biological replicates.
733 **Fig. 3** Higher expression of *ahpC* provides resistance to peroxides in *Chlamydia.* IFA of *ahpC*
734 (A) or EV (C) exposed to oxidizing agents. Construct expression was induced or not at 10 hpi
735 with 1 nM aTc, and samples were treated with three different concentrations of hydrogen
736 peroxide (H_2O_2) at 16 hpi for 30 min then fixed with methanol at 24 hpi and stained and imaged
737 as described in the legend of Fig. 2B. Representative images from three biological replicates
738 are shown. IFU analysis of *ahpC* (B) or EV (D) following treatment with oxidizing agents, CHP-
739 Cumene hydroperoxide, H_2O_2-Hydrogen peroxide, TBHP-Tert-butyl hydroperoxide, and PN-
740 Peroxynitrite. Samples were processed as described for (A) and (C), and IFUs harvested at 24
741 hpi. IFUs of treated samples were compared with respective untreated controls. ***p< 0.0001 vs
742 untreated sample by using two-way ANOVA. Data represent three biological replicates.
743 **Fig. 4** Reduced levels of AhpC negatively impact chlamydial growth. (A) Transcriptional analysis
744 of *ahpC* in knockdown (*ahpC* KD) and non-target (NT) control using RT-qPCR following
745 induction at 10 hpi with 1 nM aTc. RNA and gDNA were harvested at 14 and 24 hpi. Quantified
746 cDNA was normalized to gDNA, and values were plotted on a log scale. ***p< 0.0001 vs
747 uninduced sample by using two-way ANOVA. Data represent three biological replicates. (B) IFA

748 was performed to assess inclusion size and morphology using the same induction conditions as
749 in section (A). At 24 hpi, cells were fixed with methanol and stained using primary antibodies to
750 major outer membrane protein (MOMP), Cpf1 (dCas12), and DAPI. All images were acquired on
751 Zeiss Axio Imager Z.2 with Apotome2 at 100x magnification. Bars, 2 μm. Representative images
752 of three biological replicates are shown. (C) Quantification of genomic DNA (gDNA) determined
753 by qPCR in *ahpC* KD and NT strains. dCas12 expression was induced or not at 10 hpi, and
754 gDNA was harvested at 14 and 24 hpi and plotted on a log scale. ***p< 0.0001 vs uninduced
755 sample by using two-way ANOVA. Data represent three biological replicates. (D) IFU titers
756 following induction at 10 hpi with 1 nM aTc. IFUs were counted from 24 and 48 hpi samples and
757 calculated as percentage of uninduced samples. ***p< 0.0001, **p< 0.001 vs uninduced sample
758 by using multiple paired t test. Data represent three biological replicates. (E) Intracellular ROS
759 levels were measured to investigate the function of AhpC in reducing ROS. HeLa cells were
760 infected or not with *ahpC* knockdown, and knockdown was induced or not at 10 hpi with 1 nM
761 aTc. At 24 hpi, samples were washed with DPBS and incubated with CellROX Deep red dye for
762 30 min in dark. ROS levels were measured at wavelengths of 640nm (excitation) and 665nm
763 (emission). **p< 0.001, *p< 0.01 vs uninduced sample by using two-way ANOVA. Data
764 represent three biological replicates.

765 **Fig. 5** *Chlamydia* is hypersensitive to oxidizing agents in *ahpC* knockdown condition. IFA of
766 *ahpC* KD (A) or NT (C) treated with 62.5 μM H_2O_2. dCas12 expression was induced or not at 10
767 hpi with 1 nM aTc, treated or not with H_2O_2 at 16 hpi for 30 min, and allowed to grow until 24 hpi.
768 Coverslips were fixed with methanol at 24 hpi and stained major outer membrane protein
769 (MOMP), Cpf1 (dCas12), and DAPI. Scale bars = 2 μm. Images were captured using a Zeiss
770 Axio Imager Z.2 with Apotome2 at 100x magnification. Representative images from three
771 biological replicates are shown. IFU analysis of *ahpC* KD (B) or NT (D) following treatment with
772 oxidizing agents, CHP-Cumene hydroperoxide, H_2O_2-Hydrogen peroxide, TBHP-Tert-butyl

773 hydroperoxide, or PN-Peroxynitrite. dCas12 expression was induced or not, and samples were
774 treated or not as mentioned in the legend of Fig. 3B. IFUs of treated samples were calculated as
775 percentage of respective untreated samples. ***p< 0.0001 vs untreated sample by using two-
776 way ANOVA. Data represent three biological replicates.

777 **Fig. 6** Complementation of the phenotypes observed in the *ahpC* knockdown. (A) Confirmation
778 of complementation (comp) of *ahpC* knockdown by RT-qPCR. Samples were processed and
779 quantified as mentioned previously in the legend of Fig. 4A. Values were plotted on a log scale.
780 *p< 0.01 vs uninduced sample using ordinary one-way ANOVA. Data represent three biological
781 replicates. (B) IFA of comp strain was performed at 24 hpi, and staining and imaging were
782 performed as mentioned in the legend of Fig. 4B. Scale bars, 2 μm. Representative images from
783 three biological replicates are shown. (C) Genomic DNA quantitation was performed by qPCR.
784 Construct expression was induced or not at 10 hpi, and gDNA was harvested at 14 and 24 hpi
785 and plotted on a log scale. Statistical analysis was calculated using ordinary one-way ANOVA.
786 Data represent three biological replicates. (D) IFU analysis of comp strain. Statistical analysis
787 was calculated using multiple paired t test. Data represent three biological replicates. (E) IFA of
788 comp strain following treatment with 62.5 μM H_2O_2. Samples were treated, stained, and images
789 acquired as mentioned in the legend of Fig. 5A. Scale bars = 2 μm. Representative images from
790 three biological replicates are shown. (F) IFU analysis of comp strain following treatment with
791 oxidizing agents. Experiments were performed as mentioned in the legend of Fig. 5B. IFUs were
792 calculated as percentage of respective untreated samples. ***p< 0.0001 vs untreated sample by
793 using two-way ANOVA. Data represent three biological replicates. (G) *ahpC* knockdown growth
794 defect rescued by ROS scavengers. IFU analysis of *ahpC* knockdown treated with or without
795 scavengers, α-Tocopherol (100 μM) and DMTU (10 mM), as mentioned in materials and
796 methods. IFUs were calculated as a percentage of the untreated, uninduced sample. ***p<
797 0.0001 vs untreated, uninduced or induced sample by using two-way ANOVA. Data represent

798 three biological replicates. (H) IFA of *ahpC* knockdown treated with or without scavengers.
799 Experimental conditions were similar as in section (G). Staining and imaging were performed as
800 mentioned in Fig. 5A. Representative images from three biological replicates are shown.

801 **Fig. 7** Effects of *ahpC* knockdown/overexpression on chlamydial developmental cycle
802 progression. RT-qPCR analysis of late cycle genes (*hctA*, *hctB*, *omcB*, *tsp*, and *glgA*) in (A)
803 *ahpC* knockdown, (C) complementation, and (D) *ahpC* overexpression strain. Experimental
804 conditions were the same as mentioned in the legend of Fig. 4A. Quantified cDNA was
805 normalized to gDNA, and values were plotted on a log scale. ***$p < 0.0001$, **$p < 0.001$, *$p < 0.01$
806 vs uninduced sample by using two-way ANOVA. Data represent three biological replicates. (B)
807 One-step growth curve of *ahpC* knockdown. Samples were induced or not with 1 nM aTc at 10
808 hpi and harvested at 16, 18, 20, 22, and 24 hpi. IFUs recovered are displayed as log10 values.
809 ***$p < 0.0001$ vs uninduced sample by using two-way ANOVA. Data represent three biological
810 replicates.

811 **Fig. 8** Altering the activity of AhpC in *Ctr* L2 impacts its developmental cycle progression. (Top)
812 In *Chlamydia*, secondary differentiation is asynchronous and RBs divide through an asymmetric
813 budding mechanism. In such conditions, either the mother or daughter cell may inherit more
814 oxidized proteins (represented by a darker shade), which can then impact whether a given RB
815 will divide again or undergo secondary differentiation. (Bottom) The black dots represent EBs,
816 the orange circles show RBs. The developmental cycle of wild-type *C. trachomatis* (Ctr L2) is
817 shown. In *ahpC* KD, highly oxidized conditions lead some RBs to cross the oxidative threshold
818 sooner, allowing activation of late genes and secondary differentiation earlier than other RBs. In
819 *ahpC* overexpression, a reducing environment results in a delay in achieving the oxidative
820 threshold, thus allowing RBs to continue to divide before committing to secondary
821 differentiation.

822

823 **Supplementary Information**

824 **Table S1** List of plasmids, strains, and primers used in this study.

825 **Fig. S1** Viability assay of uninfected or infected HeLa cells treated with oxidizing agents H_2O_2
826 (A), CHP (B), TBHP (C), and PN (D). HeLa cells were infected or not with empty vector control,
827 pBOMBDC.ev (EV), and treated or not with different concentrations of oxidizing agents at 16 hpi
828 for 30 min. At 24 hpi, an end point viability assay was performed using PrestoBlue as mentioned
829 in materials and methods. The treated values were expressed as a percentage of the untreated
830 values, which were considered as 100%. Data represent three biological replicates.

831 **Fig. S2** Response of *C. trachomatis* L2 against oxidizing agents. (A) IFA of wild-type *Ctr* L2
832 exposed to oxidizing agents. Oxidizing agents' treatment, staining, and imaging were performed
833 as mentioned in materials and methods. Representative images from three biological replicates
834 are shown. (B) IFU analysis of *Ctr* L2 post-exposure with oxidizing agents. Conditions were
835 same as in section (A), and IFUs were harvested at 24 hpi. IFUs were calculated as percentage
836 of untreated samples. ***$p < 0.0001$ vs untreated sample by using one way ANOVA. Data
837 represent three biological replicates.

838 **Fig. S3** Overexpression of *ahpC* provides resistance to peroxides in *Chlamydia.* IFA of *ahpC* (A)
839 or EV (B) exposed to oxidizing agents (CHP, TBHP, and PN). Experiments were performed as
840 mentioned in the legend of Fig. 3A. Representative images from three biological replicates are
841 shown.

842 **Fig. S4** *Chlamydia* is hypersensitive to oxidizing agents as a result of reduced levels of *ahpC*.
843 IFA of *ahpC* KD (A), NT (B), comp (C) treated with CHP, TBHP, and PN. Experimental
844 conditions were the same as mentioned in the legend of Fig. 5A. Representative images from
845 three biological replicates are shown.

846 **Fig. S5** Rescue of oxidative stress phenotype by ROS scavengers in *C. trachomatis* L2. (A) IFA
847 of wild-type *Ctr* L2 incubated or not with scavengers, α-Tocopherol (100 μM) and DMTU (10
848 mM), and treated or not with 500 μM H_2O_2 as mentioned in materials and methods.

849 Representative images from three biological replicates are shown. (B) IFU analysis of *Ctr* L2
850 grown under the same conditions as mentioned in the legend of Fig. 6G. IFUs were calculated
851 as percentage of untreated samples. ***p< 0.0001, statistical analysis was performed using
852 ordinary one-way ANOVA. H_2O_2 treated sample and samples incubated with scavengers only
853 were compared to the untreated control. Samples treated with H_2O_2 and incubated with
854 scavengers were compared with sample treated with H_2O_2. Data represent three biological
855 replicates. Only significant differences are noted.

856 **Fig. S6** Effect of penicillin treatment during *ahpC* knockdown. (A) IFA was performed to assess
857 inclusion size and morphology of *ahpC* KD-spec following induction (1 nM aTc) and penicillin
858 treatment (1 U/mL) at 10 hpi. At 24 hpi, cells were fixed with methanol and stained using
859 primary antibodies to major outer membrane protein (MOMP), Cpf1 (dCas12), and DAPI. All
860 images were acquired on Zeiss Axio Imager Z.2 with Apotome2 at 100x magnification. Bars, 2
861 μm. Representative images of three biological replicates are shown. Transcriptional analysis of
862 (B) *ahpC*, (C) *hctA*, and (D) *hctB* in *ahpC* KD-spec using RT-qPCR using the same conditions
863 as in section (A). RNA samples were harvested at 16 and 24 hpi. Quantified cDNA was
864 normalized to 16SrRNA, and values were plotted on a log scale. ***p< 0.0001, **p< 0.001, *p<
865 0.01 vs uninduced sample by using two-way ANOVA. Data represent three biological replicates.

866

867 **REFERENCES**

868 Abdelrahman, Y., Ouellette, S. P., Belland, R. J., & Cox, J. V. (2016). Polarized Cell Division of
869 Chlamydia trachomatis. *PLoS Pathog*, *12*(8), e1005822.
870 https://doi.org/10.1371/journal.ppat.1005822
871 Abdelrahman, Y. M., & Belland, R. J. (2005). The chlamydial developmental cycle. *FEMS*
872 *Microbiol Rev*, *29*(5), 949-959. https://doi.org/10.1016/j.femsre.2005.03.002
873 Abdul-Sater, A. A., Said-Sadier, N., Lam, V. M., Singh, B., Pettengill, M. A., Soares, F., Tattoli, I.,
874 Lipinski, S., Girardin, S. E., Rosenstiel, P., & Ojcius, D. M. (2010). Enhancement of reactive
875 oxygen species production and chlamydial infection by the mitochondrial Nod-like family
876 member NLRX1. *J Biol Chem*, *285*(53), 41637-41645.
877 https://doi.org/10.1074/jbc.M110.137885

878 Antelmann, H., Engelmann, S., Schmid, R., & Hecker, M. (1996). General and oxidative stress
879 responses in Bacillus subtilis: cloning, expression, and mutation of the alkyl
880 hydroperoxide reductase operon. *J Bacteriol*, *178*(22), 6571-6578.
881 https://doi.org/10.1128/jb.178.22.6571-6578.1996
882 Barbour, A. G., Amano, K., Hackstadt, T., Perry, L., & Caldwell, H. D. (1982). Chlamydia
883 trachomatis has penicillin-binding proteins but not detectable muramic acid. *J Bacteriol*,
884 *151*(1), 420-428. https://doi.org/10.1128/jb.151.1.420-428.1982
885 Belland, R. J., Zhong, G., Crane, D. D., Hogan, D., Sturdevant, D., Sharma, J., Beatty, W. L., &
886 Caldwell, H. D. (2003). Genomic transcriptional profiling of the developmental cycle of
887 Chlamydia trachomatis. *Proc Natl Acad Sci U S A*, *100*(14), 8478-8483.
888 https://doi.org/10.1073/pnas.1331135100
889 Betts-Hampikian, H. J., & Fields, K. A. (2011). Disulfide bonding within components of the
890 Chlamydia type III secretion apparatus correlates with development. *J Bacteriol*, *193*(24),
891 6950-6959. https://doi.org/10.1128/JB.05163-11
892 Boncompain, G., Muller, C., Meas-Yedid, V., Schmitt-Kopplin, P., Lazarow, P. B., & Subtil, A.
893 (2014). The intracellular bacteria Chlamydia hijack peroxisomes and utilize their
894 enzymatic capacity to produce bacteria-specific phospholipids. *PLoS One*, *9*(1), e86196.
895 https://doi.org/10.1371/journal.pone.0086196
896 Boncompain, G., Schneider, B., Delevoye, C., Kellermann, O., Dautry-Varsat, A., & Subtil, A.
897 (2010). Production of reactive oxygen species is turned on and rapidly shut down in
898 epithelial cells infected with Chlamydia trachomatis. *Infect Immun*, *78*(1), 80-87.
899 https://doi.org/10.1128/IAI.00725-09
900 Brinkworth, A. J., Wildung, M. R., & Carabeo, R. A. (2018). Genomewide Transcriptional
901 Responses of Iron-Starved Chlamydia trachomatis Reveal Prioritization of Metabolic
902 Precursor Synthesis over Protein Translation. *mSystems*, *3*(1).
903 https://doi.org/10.1128/mSystems.00184-17
904 Caldwell, H. D., Kromhout, J., & Schachter, J. (1981). Purification and partial characterization of
905 the major outer membrane protein of Chlamydia trachomatis. *Infect Immun*, *31*(3),
906 1161-1176. https://doi.org/10.1128/iai.31.3.1161-1176.1981
907 Chiarelli, T. J., Grieshaber, N. A., Omsland, A., Remien, C. H., & Grieshaber, S. S. (2020). Single-
908 Inclusion Kinetics of Chlamydia trachomatis Development. *mSystems*, *5*(5).
909 https://doi.org/10.1128/mSystems.00689-20
910 Clifton, D. R., Dooley, C. A., Grieshaber, S. S., Carabeo, R. A., Fields, K. A., & Hackstadt, T. (2005).
911 Tyrosine phosphorylation of the chlamydial effector protein Tarp is species specific and
912 not required for recruitment of actin. *Infect Immun*, *73*(7), 3860-3868.
913 https://doi.org/10.1128/IAI.73.7.3860-3868.2005
914 Cosgrove, K., Coutts, G., Jonsson, I. M., Tarkowski, A., Kokai-Kun, J. F., Mond, J. J., & Foster, S. J.
915 (2007). Catalase (KatA) and alkyl hydroperoxide reductase (AhpC) have compensatory
916 roles in peroxide stress resistance and are required for survival, persistence, and nasal
917 colonization in Staphylococcus aureus. *J Bacteriol*, *189*(3), 1025-1035.
918 https://doi.org/10.1128/JB.01524-06
919 Cox, J. V., Abdelrahman, Y. M., & Ouellette, S. P. (2020). Penicillin-binding proteins regulate
920 multiple steps in the polarized cell division process of Chlamydia. *Sci Rep*, *10*(1), 12588.
921 https://doi.org/10.1038/s41598-020-69397-x

922 de Oliveira, M. A., Tairum, C. A., Netto, L. E. S., de Oliveira, A. L. P., Aleixo-Silva, R. L., Cabrera, V.
923 I. M., Breyer, C. A., & Dos Santos, M. C. (2021). Relevance of peroxiredoxins in
924 pathogenic microorganisms. *Appl Microbiol Biotechnol*, *105*(14-15), 5701-5717.
925 https://doi.org/10.1007/s00253-021-11360-5
926 Dip, P. V., Kamariah, N., Nartey, W., Beushausen, C., Kostyuchenko, V. A., Ng, T. S., Lok, S. M.,
927 Saw, W. G., Eisenhaber, F., Eisenhaber, B., & Gruber, G. (2014). Key roles of the
928 Escherichia coli AhpC C-terminus in assembly and catalysis of alkylhydroperoxide
929 reductase, an enzyme essential for the alleviation of oxidative stress. *Biochim Biophys*
930 *Acta*, *1837*(12), 1932-1943. https://doi.org/10.1016/j.bbabio.2014.08.007
931 Everett, K. D., & Hatch, T. P. (1995). Architecture of the cell envelope of Chlamydia psittaci 6BC. *J*
932 *Bacteriol*, *177*(4), 877-882. https://doi.org/10.1128/jb.177.4.877-882.1995
933 Ezraty, B., Gennaris, A., Barras, F., & Collet, J. F. (2017). Oxidative stress, protein damage and
934 repair in bacteria. *Nat Rev Microbiol*, *15*(7), 385-396.
935 https://doi.org/10.1038/nrmicro.2017.26
936 Fang, F. C. (2011). Antimicrobial actions of reactive oxygen species. *mBio*, *2*(5).
937 https://doi.org/10.1128/mBio.00141-11
938 Feng, X., Guo, K., & Gao, H. (2020). Plasticity of the peroxidase AhpC links multiple substrates to
939 diverse disulfide-reducing pathways in Shewanella oneidensis. *J Biol Chem*, *295*(32),
940 11118-11130. https://doi.org/10.1074/jbc.RA120.014010
941 Gehre, L., Gorgette, O., Perrinet, S., Prevost, M. C., Ducatez, M., Giebel, A. M., Nelson, D. E., Ball,
942 S. G., & Subtil, A. (2016). Sequestration of host metabolism by an intracellular pathogen.
943 *Elife*, *5*, e12552. https://doi.org/10.7554/eLife.12552
944 Gerard, H. C., Freise, J., Wang, Z., Roberts, G., Rudy, D., Krauss-Opatz, B., Kohler, L., Zeidler, H.,
945 Schumacher, H. R., Whittum-Hudson, J. A., & Hudson, A. P. (2002). Chlamydia
946 trachomatis genes whose products are related to energy metabolism are expressed
947 differentially in active vs. persistent infection. *Microbes Infect*, *4*(1), 13-22.
948 https://doi.org/10.1016/s1286-4579(01)01504-0
949 Hatch, N. D., & Ouellette, S. P. (2023). Identification of the alternative sigma factor regulons of
950 Chlamydia trachomatis using multiplexed CRISPR interference. *mSphere*, *8*(5), e0039123.
951 https://doi.org/10.1128/msphere.00391-23
952 Hollander-Czytko, H., Grabowski, J., Sandorf, I., Weckermann, K., & Weiler, E. W. (2005).
953 Tocopherol content and activities of tyrosine aminotransferase and cystine lyase in
954 Arabidopsis under stress conditions. *J Plant Physiol*, *162*(7), 767-770.
955 https://doi.org/10.1016/j.jplph.2005.04.019
956 Iliffe-Lee, E. R., & McClarty, G. (1999). Glucose metabolism in Chlamydia trachomatis: the
957 'energy parasite' hypothesis revisited. *Mol Microbiol*, *33*(1), 177-187.
958 https://doi.org/10.1046/j.1365-2958.1999.01464.x
959 Kiffin, R., Bandyopadhyay, U., & Cuervo, A. M. (2006). Oxidative stress and autophagy. *Antioxid*
960 *Redox Signal*, *8*(1-2), 152-162. https://doi.org/10.1089/ars.2006.8.152
961 Kimura, A., Yuhara, S., Ohtsubo, Y., Nagata, Y., & Tsuda, M. (2012). Suppression of pleiotropic
962 phenotypes of a Burkholderia multivorans fur mutant by oxyR mutation. *Microbiology*
963 *(Reading)*, *158*(Pt 5), 1284-1293. https://doi.org/10.1099/mic.0.057372-0

964 Koshkin, A., Knudsen, G. M., & Ortiz De Montellano, P. R. (2004). Intermolecular interactions in
965 the AhpC/AhpD antioxidant defense system of Mycobacterium tuberculosis. *Arch*
966 *Biochem Biophys*, *427*(1), 41-47. https://doi.org/10.1016/j.abb.2004.04.017
967 Lee, J., Cox, J. V., & Ouellette, S. P. (2020). Critical Role for the Extended N Terminus of
968 Chlamydial MreB in Directing Its Membrane Association and Potential Interaction with
969 Divisome Proteins. *J Bacteriol*, *202*(9). https://doi.org/10.1128/JB.00034-20
970 Loprasert, S., Sallabhan, R., Whangsuk, W., & Mongkolsuk, S. (2003). Compensatory increase in
971 ahpC gene expression and its role in protecting Burkholderia pseudomallei against
972 reactive nitrogen intermediates. *Arch Microbiol*, *180*(6), 498-502.
973 https://doi.org/10.1007/s00203-003-0621-9
974 Mastronicola, D., Falabella, M., Testa, F., Pucillo, L. P., Teixeira, M., Sarti, P., Saraiva, L. M., &
975 Giuffre, A. (2014). Functional characterization of peroxiredoxins from the human
976 protozoan parasite Giardia intestinalis. *PLoS Negl Trop Dis*, *8*(1), e2631.
977 https://doi.org/10.1371/journal.pntd.0002631
978 Matsumoto, A., & Manire, G. P. (1970). Electron Microscopic Observations on the Fine Structure
979 of Cell Walls of Chlamydia psittaci. *J Bacteriol*, *104*(3), 1332-1337.
980 https://doi.org/10.1128/jb.104.3.1332-1337.1970
981 Mishra, S., & Imlay, J. (2012). Why do bacteria use so many enzymes to scavenge hydrogen
982 peroxide? *Arch Biochem Biophys*, *525*(2), 145-160.
983 https://doi.org/10.1016/j.abb.2012.04.014
984 Mongkolsuk, S., Whangsuk, W., Vattanaviboon, P., Loprasert, S., & Fuangthong, M. (2000). A
985 Xanthomonas alkyl hydroperoxide reductase subunit C (ahpC) mutant showed an altered
986 peroxide stress response and complex regulation of the compensatory response of
987 peroxide detoxification enzymes. *J Bacteriol*, *182*(23), 6845-6849.
988 https://doi.org/10.1128/JB.182.23.6845-6849.2000
989 Moulder, J. W. (1993). Why is Chlamydia sensitive to penicillin in the absence of peptidoglycan?
990 *Infect Agents Dis*, *2*(2), 87-99. https://www.ncbi.nlm.nih.gov/pubmed/8162358
991 Moulder, J. W., Colon, J. I., Ruda, J., & Zebovitz, M. M. (1956). The effect of penicillin on
992 multiplying and nonmultiplying populations of sensitive and resistant strains of feline
993 pneumonitis virus. *J Infect Dis*, *98*(3), 229-238. https://doi.org/10.1093/infdis/98.3.229
994 Mueller, K. E., Wolf, K., & Fields, K. A. (2017). Chlamydia trachomatis Transformation and Allelic
995 Exchange Mutagenesis. *Curr Protoc Microbiol*, *45*, 11A 13 11-11A 13 15.
996 https://doi.org/10.1002/cpmc.31
997 Mygind, P., Christiansen, G., Persson, K., & Birkelund, S. (1998). Analysis of the humoral immune
998 response to Chlamydia outer membrane protein 2. *Clin Diagn Lab Immunol*, *5*(3), 313-
999 318. https://doi.org/10.1128/CDLI.5.3.313-318.1998
1000 Newhall, W. J. t. (1987). Biosynthesis and disulfide cross-linking of outer membrane components
1001 during the growth cycle of Chlamydia trachomatis. *Infect Immun*, *55*(1), 162-168.
1002 https://doi.org/10.1128/iai.55.1.162-168.1987
1003 Ochsner, U. A., Vasil, M. L., Alsabbagh, E., Parvatiyar, K., & Hassett, D. J. (2000). Role of the
1004 Pseudomonas aeruginosa oxyR-recG operon in oxidative stress defense and DNA repair:
1005 OxyR-dependent regulation of katB-ankB, ahpB, and ahpC-ahpF. *J Bacteriol*, *182*(16),
1006 4533-4544. https://doi.org/10.1128/JB.182.16.4533-4544.2000

1007 Oh, E., & Jeon, B. (2014). Role of alkyl hydroperoxide reductase (AhpC) in the biofilm formation
1008 of Campylobacter jejuni. *PLoS One*, *9*(1), e87312.
1009 https://doi.org/10.1371/journal.pone.0087312
1010 Ouellette, S. P. (2018). Feasibility of a Conditional Knockout System for Chlamydia Based on
1011 CRISPR Interference. *Front Cell Infect Microbiol*, *8*, 59.
1012 https://doi.org/10.3389/fcimb.2018.00059
1013 Ouellette, S. P., Blay, E. A., Hatch, N. D., & Fisher-Marvin, L. A. (2021). CRISPR Interference To
1014 Inducibly Repress Gene Expression in Chlamydia trachomatis. *Infect Immun*, *89*(7),
1015 e0010821. https://doi.org/10.1128/IAI.00108-21
1016 Ouellette, S. P., Fisher-Marvin, L. A., Harpring, M., Lee, J., Rucks, E. A., & Cox, J. V. (2022).
1017 Localized cardiolipin synthesis is required for the assembly of MreB during the polarized
1018 cell division of Chlamydia trachomatis. *PLoS Pathog*, *18*(9), e1010836.
1019 https://doi.org/10.1371/journal.ppat.1010836
1020 Ouellette, S. P., Hatch, T. P., AbdelRahman, Y. M., Rose, L. A., Belland, R. J., & Byrne, G. I. (2006).
1021 Global transcriptional upregulation in the absence of increased translation in Chlamydia
1022 during IFNgamma-mediated host cell tryptophan starvation. *Mol Microbiol*, *62*(5), 1387-
1023 1401. https://doi.org/10.1111/j.1365-2958.2006.05465.x
1024 Ouellette, S. P., Karimova, G., Subtil, A., & Ladant, D. (2012). Chlamydia co-opts the rod shape-
1025 determining proteins MreB and Pbp2 for cell division. *Mol Microbiol*, *85*(1), 164-178.
1026 https://doi.org/10.1111/j.1365-2958.2012.08100.x
1027 Ouellette, S. P., Lee, J., & Cox, J. V. (2020). Division without Binary Fission: Cell Division in the
1028 FtsZ-Less Chlamydia. *J Bacteriol*, *202*(17). https://doi.org/10.1128/JB.00252-20
1029 Pan, S., Jensen, A. A., Wood, N. A., Henrichfreise, B., Brotz-Oesterhelt, H., Fisher, D. J., Sass, P., &
1030 Ouellette, S. P. (2023). Molecular Characterization of the ClpC AAA+ ATPase in the
1031 Biology of Chlamydia trachomatis. *mBio*, *14*(2), e0007523.
1032 https://doi.org/10.1128/mbio.00075-23
1033 Panzetta, M. E., Valdivia, R. H., & Saka, H. A. (2018). Chlamydia Persistence: A Survival Strategy
1034 to Evade Antimicrobial Effects in-vitro and in-vivo. *Front Microbiol*, *9*, 3101.
1035 https://doi.org/10.3389/fmicb.2018.03101
1036 Parsonage, D., Karplus, P. A., & Poole, L. B. (2008). Substrate specificity and redox potential of
1037 AhpC, a bacterial peroxiredoxin. *Proc Natl Acad Sci U S A*, *105*(24), 8209-8214.
1038 https://doi.org/10.1073/pnas.0708308105
1039 Pokorzynski, N. D., Brinkworth, A. J., & Carabeo, R. (2019). A bipartite iron-dependent
1040 transcriptional regulation of the tryptophan salvage pathway in Chlamydia trachomatis.
1041 *Elife*, *8*. https://doi.org/10.7554/eLife.42295
1042 Poole, L. B., & Ellis, H. R. (1996). Flavin-dependent alkyl hydroperoxide reductase from
1043 Salmonella typhimurium. 1. Purification and enzymatic activities of overexpressed AhpF
1044 and AhpC proteins. *Biochemistry*, *35*(1), 56-64. https://doi.org/10.1021/bi951887s
1045 Reuter, J., Otten, C., Jacquier, N., Lee, J., Mengin-Lecreulx, D., Lockener, I., Kluj, R., Mayer, C.,
1046 Corona, F., Dannenberg, J., Aeby, S., Buhl, H., Greub, G., Vollmer, W., Ouellette, S. P.,
1047 Schneider, T., & Henrichfreise, B. (2023). An NlpC/P60 protein catalyzes a key step in
1048 peptidoglycan recycling at the intersection of energy recovery, cell division and immune
1049 evasion in the intracellular pathogen Chlamydia trachomatis. *PLoS Pathog*, *19*(2),
1050 e1011047. https://doi.org/10.1371/journal.ppat.1011047

1051 Richard, D., Bartfai, R., Volz, J., Ralph, S. A., Muller, S., Stunnenberg, H. G., & Cowman, A. F.
1052 (2011). A genome-wide chromatin-associated nuclear peroxiredoxin from the malaria
1053 parasite Plasmodium falciparum. *J Biol Chem*, *286*(13), 11746-11755.
1054 https://doi.org/10.1074/jbc.M110.198499
1055 Rusconi, B., & Greub, G. (2013). Discovery of catalases in members of the Chlamydiales order. *J*
1056 *Bacteriol*, *195*(16), 3543-3551. https://doi.org/10.1128/JB.00563-13
1057 Seaver, L. C., & Imlay, J. A. (2001). Alkyl hydroperoxide reductase is the primary scavenger of
1058 endogenous hydrogen peroxide in Escherichia coli. *J Bacteriol*, *183*(24), 7173-7181.
1059 https://doi.org/10.1128/JB.183.24.7173-7181.2001
1060 Sherman, D. R., Mdluli, K., Hickey, M. J., Barry, C. E., 3rd, & Stover, C. K. (1999). AhpC, oxidative
1061 stress and drug resistance in Mycobacterium tuberculosis. *Biofactors*, *10*(2-3), 211-217.
1062 https://doi.org/10.1002/biof.5520100219
1063 Soules, K. R., Dmitriev, A., LaBrie, S. D., Dimond, Z. E., May, B. H., Johnson, D. K., Zhang, Y.,
1064 Battaile, K. P., Lovell, S., & Hefty, P. S. (2020). Structural and ligand binding analyses of
1065 the periplasmic sensor domain of RsbU in Chlamydia trachomatis support a role in TCA
1066 cycle regulation. *Mol Microbiol*, *113*(1), 68-88. https://doi.org/10.1111/mmi.14401
1067 Soules, K. R., LaBrie, S. D., May, B. H., & Hefty, P. S. (2020). Sigma 54-Regulated Transcription Is
1068 Associated with Membrane Reorganization and Type III Secretion Effectors during
1069 Conversion to Infectious Forms of Chlamydia trachomatis. *mBio*, *11*(5).
1070 https://doi.org/10.1128/mBio.01725-20
1071 Staerck, C., Gastebois, A., Vandeputte, P., Calenda, A., Larcher, G., Gillmann, L., Papon, N.,
1072 Bouchara, J. P., & Fleury, M. J. J. (2017). Microbial antioxidant defense enzymes. *Microb*
1073 *Pathog*, *110*, 56-65. https://doi.org/10.1016/j.micpath.2017.06.015
1074 Storz, G., Jacobson, F. S., Tartaglia, L. A., Morgan, R. W., Silveira, L. A., & Ames, B. N. (1989). An
1075 alkyl hydroperoxide reductase induced by oxidative stress in Salmonella typhimurium
1076 and Escherichia coli: genetic characterization and cloning of ahp. *J Bacteriol*, *171*(4),
1077 2049-2055. https://doi.org/10.1128/jb.171.4.2049-2055.1989
1078 Sun, Z., Sun, Y., Li, Y., Luan, X., Chen, H., Wu, H., Peng, B., & Lu, C. (2020). Identification of HeLa
1079 cell proteins that interact with Chlamydia trachomatis glycogen synthase using yeast
1080 two-hybrid assays. *Mol Med Rep*, *21*(3), 1572-1580.
1081 https://doi.org/10.3892/mmr.2020.10947
1082 Swoboda, A. R., Wood, N. A., Saery, E. A., Fisher, D. J., & Ouellette, S. P. (2023). The Periplasmic
1083 Tail-Specific Protease, Tsp, Is Essential for Secondary Differentiation in Chlamydia
1084 trachomatis. *J Bacteriol*, *205*(5), e0009923. https://doi.org/10.1128/jb.00099-23
1085 Thompson, C. C., Griffiths, C., Nicod, S. S., Lowden, N. M., Wigneshweraraj, S., Fisher, D. J., &
1086 McClure, M. O. (2015). The Rsb Phosphoregulatory Network Controls Availability of the
1087 Primary Sigma Factor in Chlamydia trachomatis and Influences the Kinetics of Growth
1088 and Development. *PLoS Pathog*, *11*(8), e1005125.
1089 https://doi.org/10.1371/journal.ppat.1005125
1090 Walch, M., Dotiwala, F., Mulik, S., Thiery, J., Kirchhausen, T., Clayberger, C., Krensky, A. M.,
1091 Martinvalet, D., & Lieberman, J. (2015). Cytotoxic Cells Kill Intracellular Bacteria through
1092 Granulysin-Mediated Delivery of Granzymes. *Cell*, *161*(5), 1229.
1093 https://doi.org/10.1016/j.cell.2015.05.021

1094 Wan, F., Feng, X., Yin, J., & Gao, H. (2021). Distinct H(2)O(2)-Scavenging System in Yersinia
1095 pseudotuberculosis: KatG and AhpC Act Together to Scavenge Endogenous Hydrogen
1096 Peroxide. *Front Microbiol*, *12*, 626874. https://doi.org/10.3389/fmicb.2021.626874
1097 Wang, G., Conover, R. C., Benoit, S., Olczak, A. A., Olson, J. W., Johnson, M. K., & Maier, R. J.
1098 (2004). Role of a bacterial organic hydroperoxide detoxification system in preventing
1099 catalase inactivation. *J Biol Chem*, *279*(50), 51908-51914.
1100 https://doi.org/10.1074/jbc.M408450200
1101 Wang, X., Schwarzer, C., Hybiske, K., Machen, T. E., & Stephens, R. S. (2014). Developmental
1102 stage oxidoreductive states of Chlamydia and infected host cells. *mBio*, *5*(6), e01924.
1103 https://doi.org/10.1128/mBio.01924-14
1104 Wang, Y., Kahane, S., Cutcliffe, L. T., Skilton, R. J., Lambden, P. R., & Clarke, I. N. (2011).
1105 Development of a transformation system for Chlamydia trachomatis: restoration of
1106 glycogen biosynthesis by acquisition of a plasmid shuttle vector. *PLoS Pathog*, *7*(9),
1107 e1002258. https://doi.org/10.1371/journal.ppat.1002258
1108 Wong, C. F., Shin, J., Subramanian Manimekalai, M. S., Saw, W. G., Yin, Z., Bhushan, S., Kumar, A.,
1109 Ragunathan, P., & Grüber, G. (2017). AhpC of the mycobacterial antioxidant defense
1110 system and its interaction with its reducing partner Thioredoxin-C. *Sci Rep*, *7*(1), 5159.
1111 https://doi.org/10.1038/s41598-017-05354-5
1112 Wood, N. A., Swoboda, A. R., Blocker, A. M., Fisher, D. J., & Ouellette, S. P. (2022). Tag-
1113 Dependent Substrate Selection of ClpX Underlies Secondary Differentiation of Chlamydia
1114 trachomatis. *mBio*, *13*(5), e0185822. https://doi.org/10.1128/mbio.01858-22
1115 Yang, K. S., Kang, S. W., Woo, H. A., Hwang, S. C., Chae, H. Z., Kim, K., & Rhee, S. G. (2002).
1116 Inactivation of human peroxiredoxin I during catalysis as the result of the oxidation of
1117 the catalytic site cysteine to cysteine-sulfinic acid. *J Biol Chem*, *277*(41), 38029-38036.
1118 https://doi.org/10.1074/jbc.M206626200
1119 Zhang, B., Gu, H., Yang, Y., Bai, H., Zhao, C., Si, M., Su, T., & Shen, X. (2019). Molecular
1120 Mechanisms of AhpC in Resistance to Oxidative Stress in Burkholderia thailandensis.
1121 *Front Microbiol*, *10*, 1483. https://doi.org/10.3389/fmicb.2019.01483
1122 Zuo, F., Yu, R., Khaskheli, G. B., Ma, H., Chen, L., Zeng, Z., Mao, A., & Chen, S. (2014).
1123 Homologous overexpression of alkyl hydroperoxide reductase subunit C (ahpC) protects
1124 Bifidobacterium longum strain NCC2705 from oxidative stress. *Res Microbiol*, *165*(7),
1125 581-589. https://doi.org/10.1016/j.resmic.2014.05.040
1126

(A)

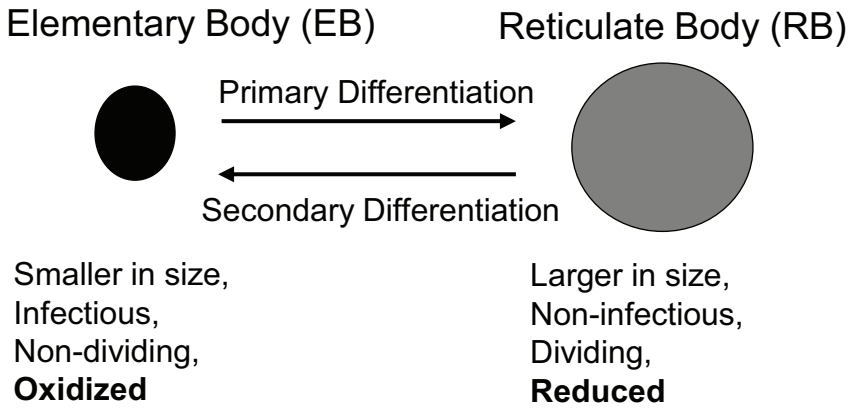
Elementary Body (EB)
Reticulate Body (RB)
Primary Differentiation
Secondary Differentiation
Smaller in size,
Infectious,
Non-dividing,
Oxidized
Larger in size,
Non-infectious,
Dividing,
Reduced

(B)

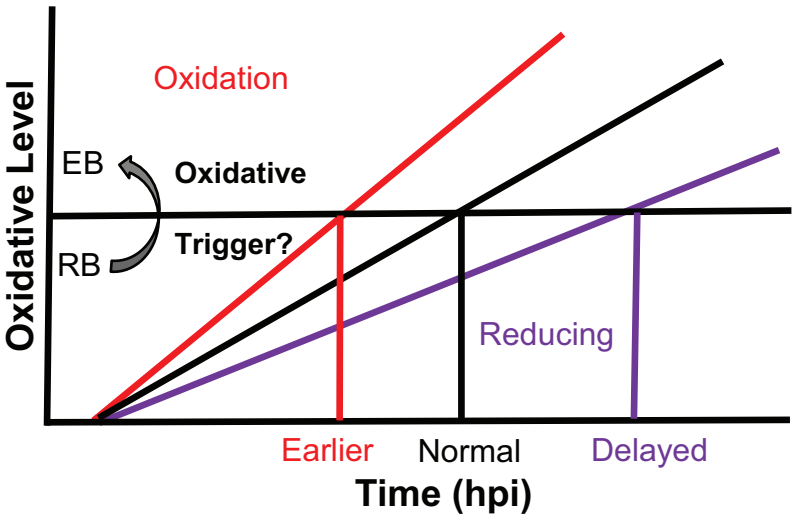
Oxidative Level
Oxidation
EB
Oxidative
Trigger?
RB
Reducing
Earlier
Normal
Delayed
Time (hpi)

(C)

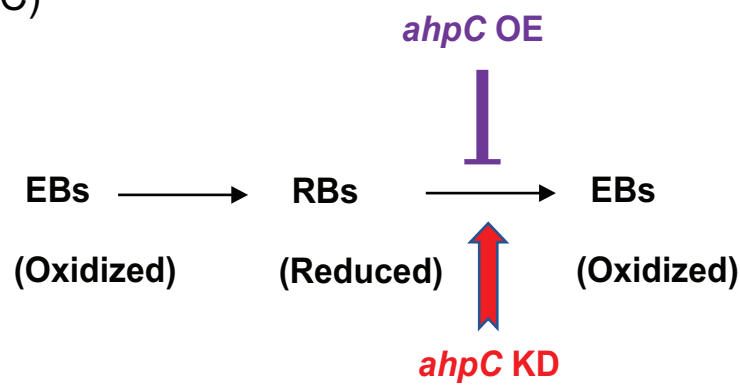
ahpC OE
EBs
(Oxidized)
RBs
(Reduced)
EBs
(Oxidized)
ahpC KD

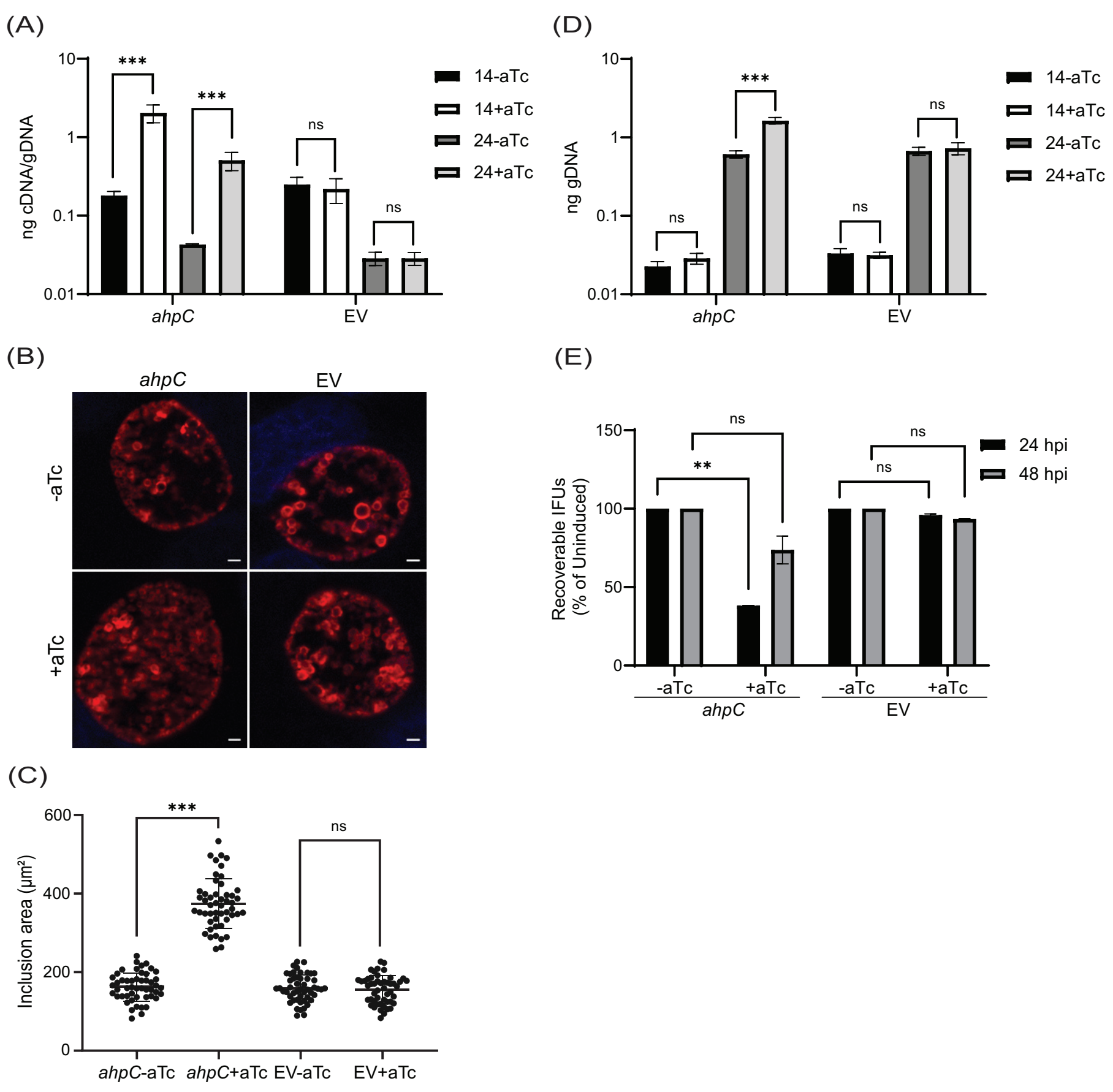
(A)
ng cDNA/gDNA
10
1
0.1
0.01
***
***
ns
ns
ahpC
EV
14-aTc
14+aTc
24-aTc
24+aTc
(D)
ng gDNA
10
1
0.1
0.01
***
ns
ns
ns
ahpC
EV
14-aTc
14+aTc
24-aTc
24+aTc
(B)
ahpC
EV
-aTc
+aTc
(E)
Recoverable IFUs
(% of Uninduced)
150
100
50
0
ns
**
ns
ns
-aTc
+aTc
-aTc
+aTc
ahpC
EV
24 hpi
48 hpi
(C)
Inclusion area (μm²)
600
400
200
0
***
ns
ahpC-aTc
ahpC+aTc
EV-aTc
EV+aTc

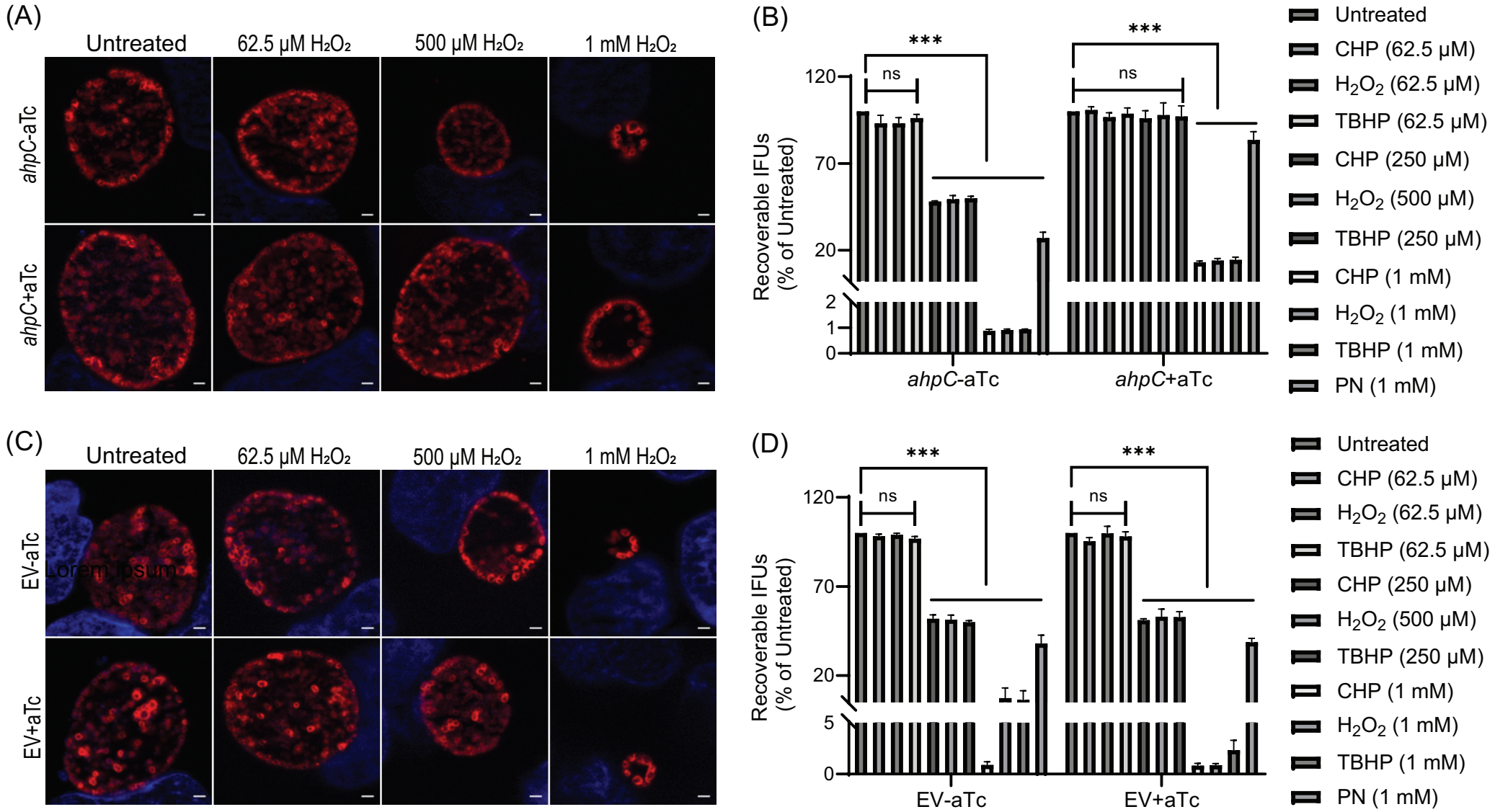
(A)
Untreated
62.5 μM H2O2
500 μM H2O2
1 mM H2O2
ahpC-aTc
ahpC+aTc
(B)
***
ns
Recoverable IFUs (% of Untreated)
120
70
20
2
1
0
ahpC-aTc
ahpC+aTc
Untreated
CHP (62.5 μM)
H2O2 (62.5 μM)
TBHP (62.5 μM)
CHP (250 μM)
H2O2 (500 μM)
TBHP (250 μM)
CHP (1 mM)
H2O2 (1 mM)
TBHP (1 mM)
PN (1 mM)
(C)
Untreated
62.5 μM H2O2
500 μM H2O2
1 mM H2O2
EV-aTc
EV+aTc
(D)
***
ns
Recoverable IFUs (% of Untreated)
120
70
20
5
0
EV-aTc
EV+aTc
Untreated
CHP (62.5 μM)
H2O2 (62.5 μM)
TBHP (62.5 μM)
CHP (250 μM)
H2O2 (500 μM)
TBHP (250 μM)
CHP (1 mM)
H2O2 (1 mM)
TBHP (1 mM)
PN (1 mM)

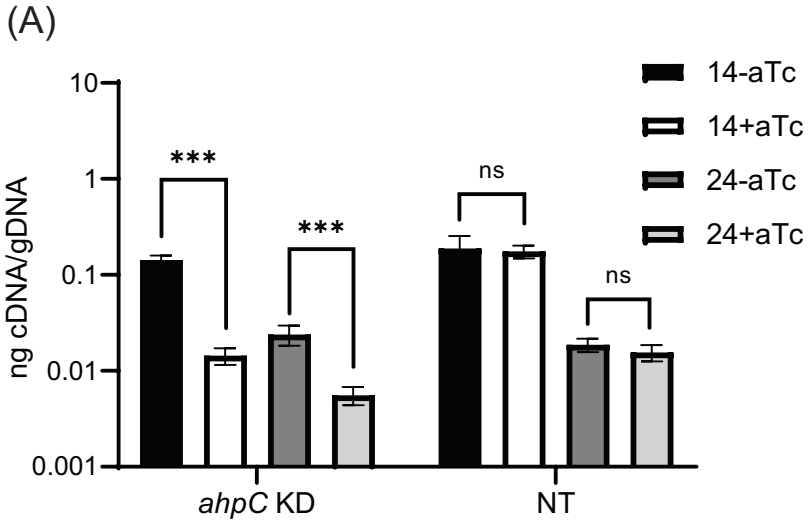
(A)
ng cDNA/gDNA
10
1
0.1
0.01
0.001
***
***
ns
ns
14-aTc
14+aTc
24-aTc
24+aTc
ahpC KD
NT

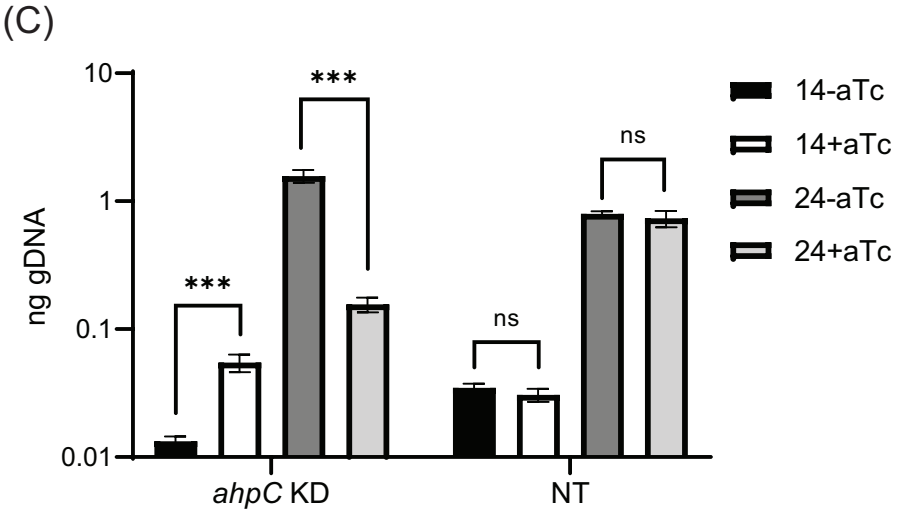
(C)
ng gDNA
10
1
0.1
0.01
***
***
ns
ns
14-aTc
14+aTc
24-aTc
24+aTc
ahpC KD
NT

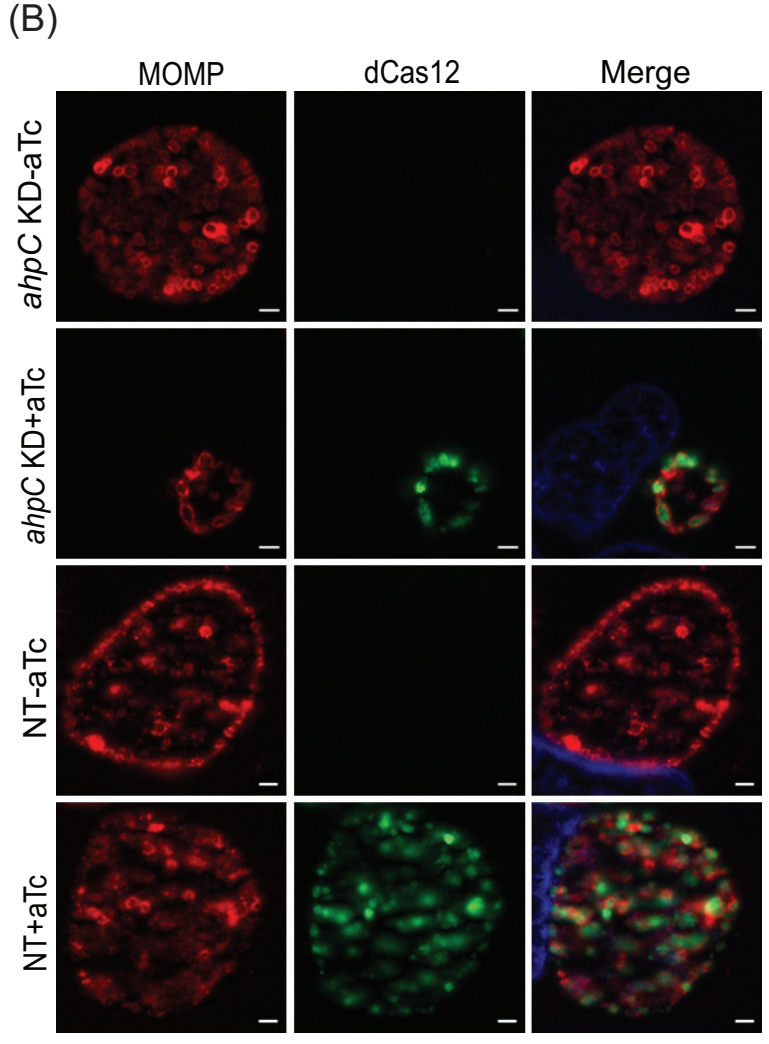
(B)
MOMP
dCas12
Merge
ahpC KD-aTc
ahpC KD+aTc
NT-aTc
NT+aTc

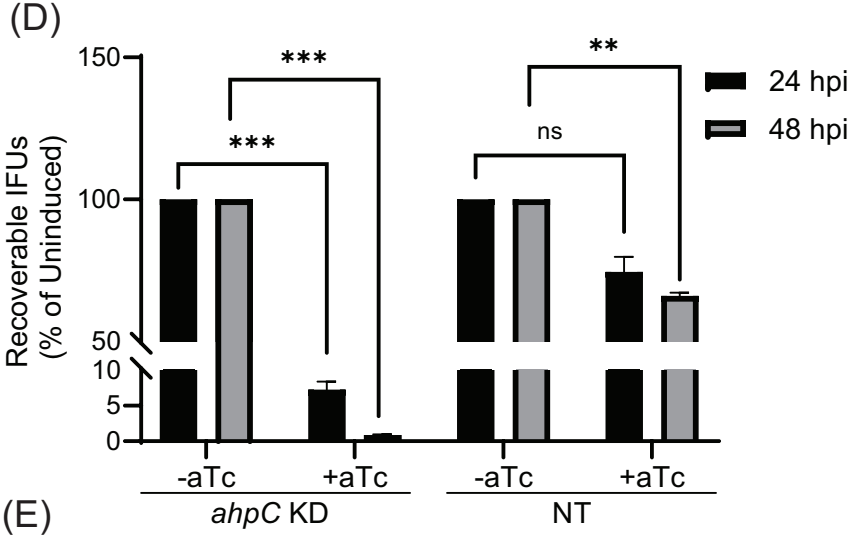
(D)
Recoverable IFUs
(% of Uninduced)
150
100
50
10
5
0
***
***
**
ns
24 hpi
48 hpi
-aTc
+aTc
-aTc
+aTc
ahpC KD
NT

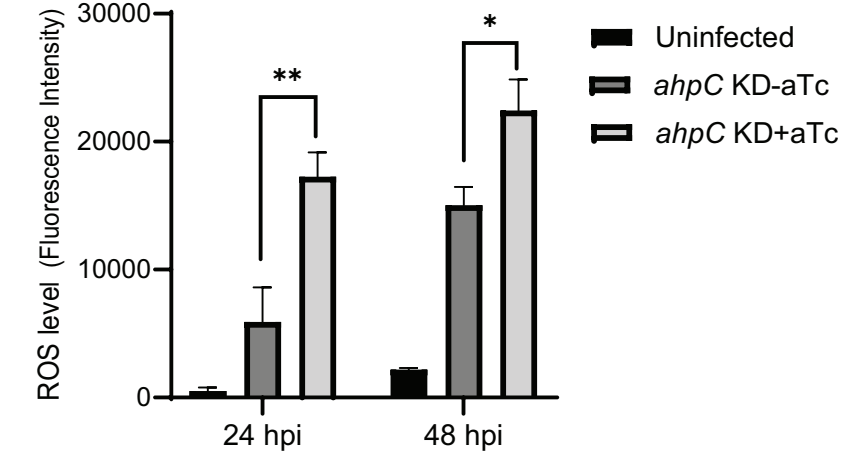
(E)
ROS level (Fluorescence Intensity)
30000
20000
10000
0
**
*
Uninfected
ahpC KD-aTc
ahpC KD+aTc
24 hpi
48 hpi

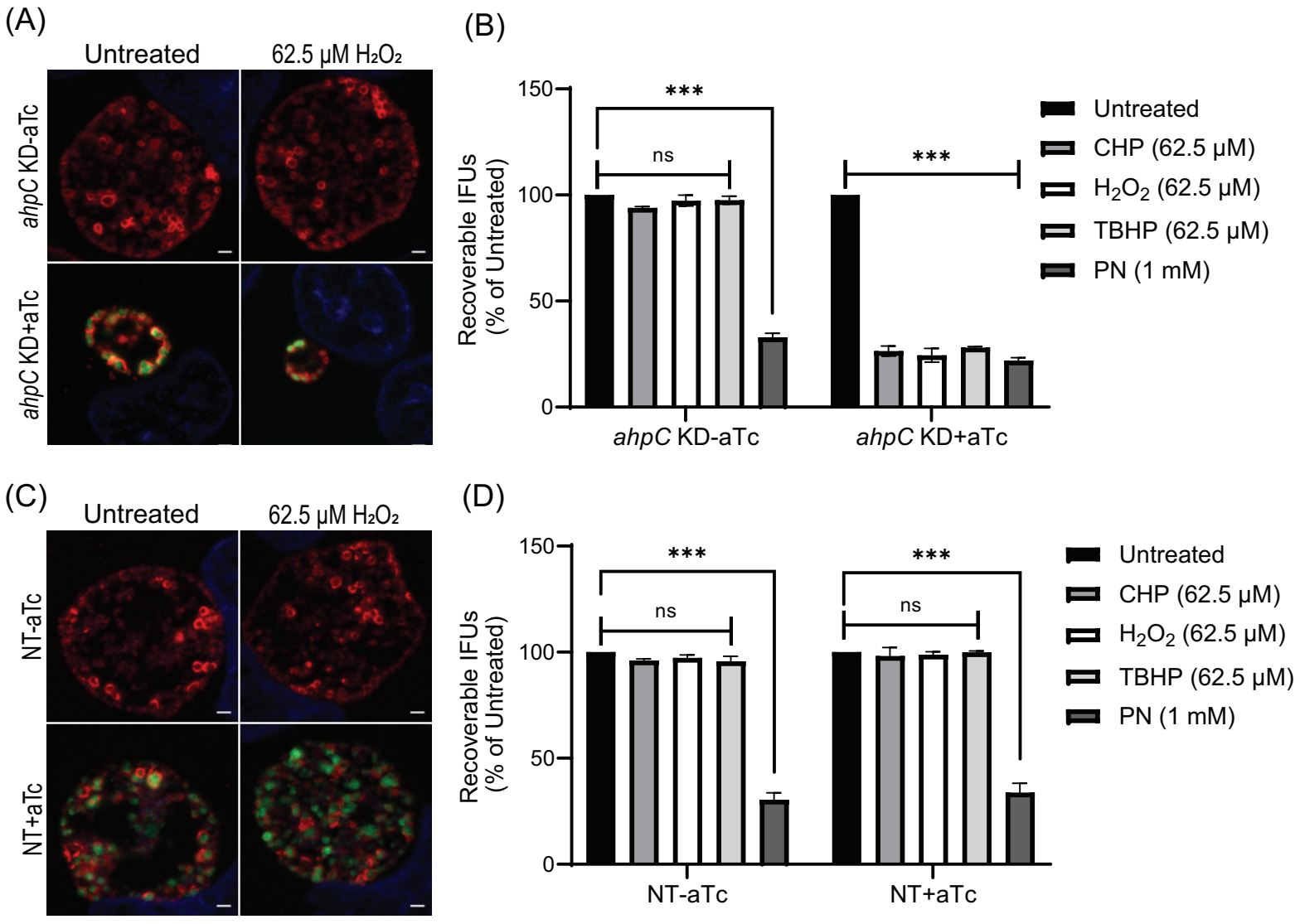
(A)
Untreated
62.5 μM H₂O₂
ahpC KD-aTc
ahpC KD+aTc
(B)
Recoverable IFUs (% of Untreated)
150
100
50
0
***
ns
***
ahpC KD-aTc
ahpC KD+aTc
Untreated
CHP (62.5 μM)
H₂O₂ (62.5 μM)
TBHP (62.5 μM)
PN (1 mM)
(C)
Untreated
62.5 μM H₂O₂
NT-aTc
NT+aTc
(D)
Recoverable IFUs (% of Untreated)
150
100
50
0
***
ns
***
ns
NT-aTc
NT+aTc
Untreated
CHP (62.5 μM)
H₂O₂ (62.5 μM)
TBHP (62.5 μM)
PN (1 mM)

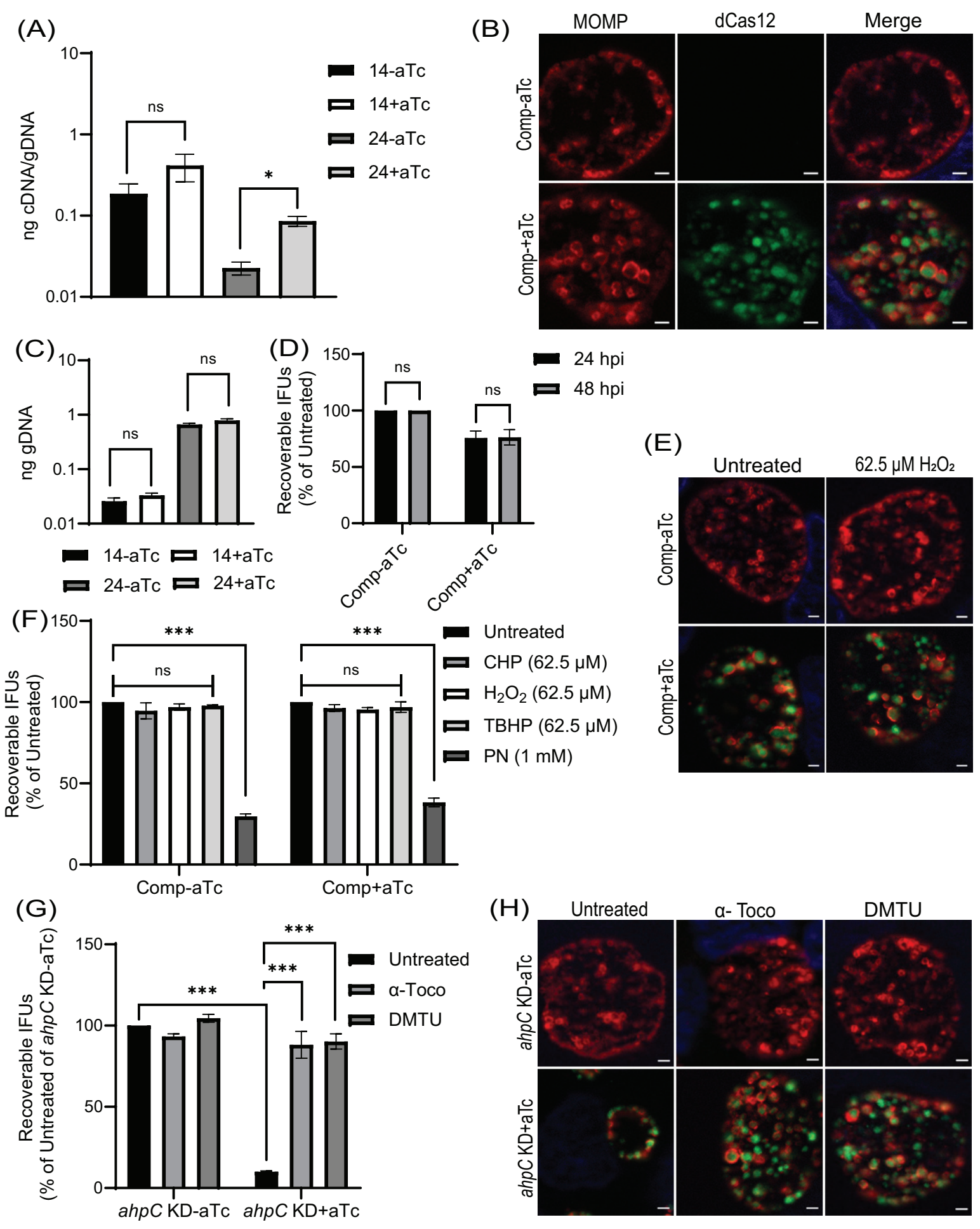
(A)
ng cDNA/gDNA
10
1
0.1
0.01
ns
*
14-aTc
14+aTc
24-aTc
24+aTc
(B)
MOMP
dCas12
Merge
Comp-aTc
Comp+aTc
(C)
ng gDNA
10
1
0.1
0.01
ns
ns
14-aTc
14+aTc
24-aTc
24+aTc
(D)
Recoverable IFUs
(% of Untreated)
150
100
50
0
ns
ns
24 hpi
48 hpi
Comp-aTc
Comp+aTc
(E)
Untreated
62.5 μM H₂O₂
Comp-aTc
Comp+aTc
(F)
Recoverable IFUs
(% of Untreated)
150
100
50
0
***
ns
***
ns
Untreated
CHP (62.5 μM)
H₂O₂ (62.5 μM)
TBHP (62.5 μM)
PN (1 mM)
Comp-aTc
Comp+aTc
(G)
Recoverable IFUs
(% of Untreated of ahpC KD-aTc)
150
100
50
0
***
***
***
Untreated
α-Toco
DMTU
ahpC KD-aTc
ahpC KD+aTc
(H)
Untreated
α- Toco
DMTU
ahpC KD-aTc
ahpC KD+aTc

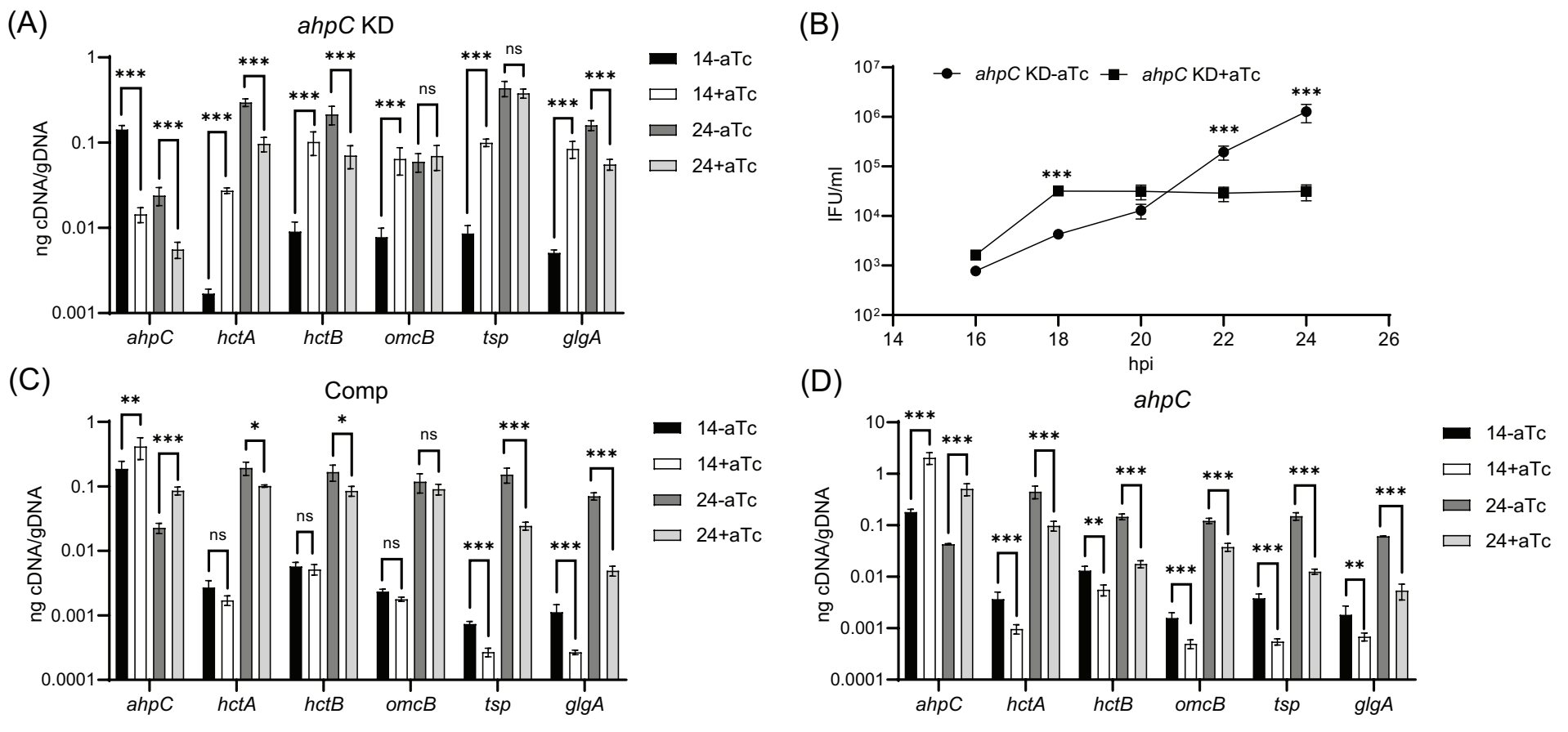
(A)
ahpC KD
ng cDNA/gDNA
1
0.1
0.01
0.001
ahpC
hctA
hctB
omcB
tsp
glgA
14-aTc
14+aTc
24-aTc
24+aTc
(B)
ahpC KD-aTc
ahpC KD+aTc
IFU/ml
hpi
(C)
Comp
ng cDNA/gDNA
0.0001
(D)
ahpC
ng cDNA/gDNA
10

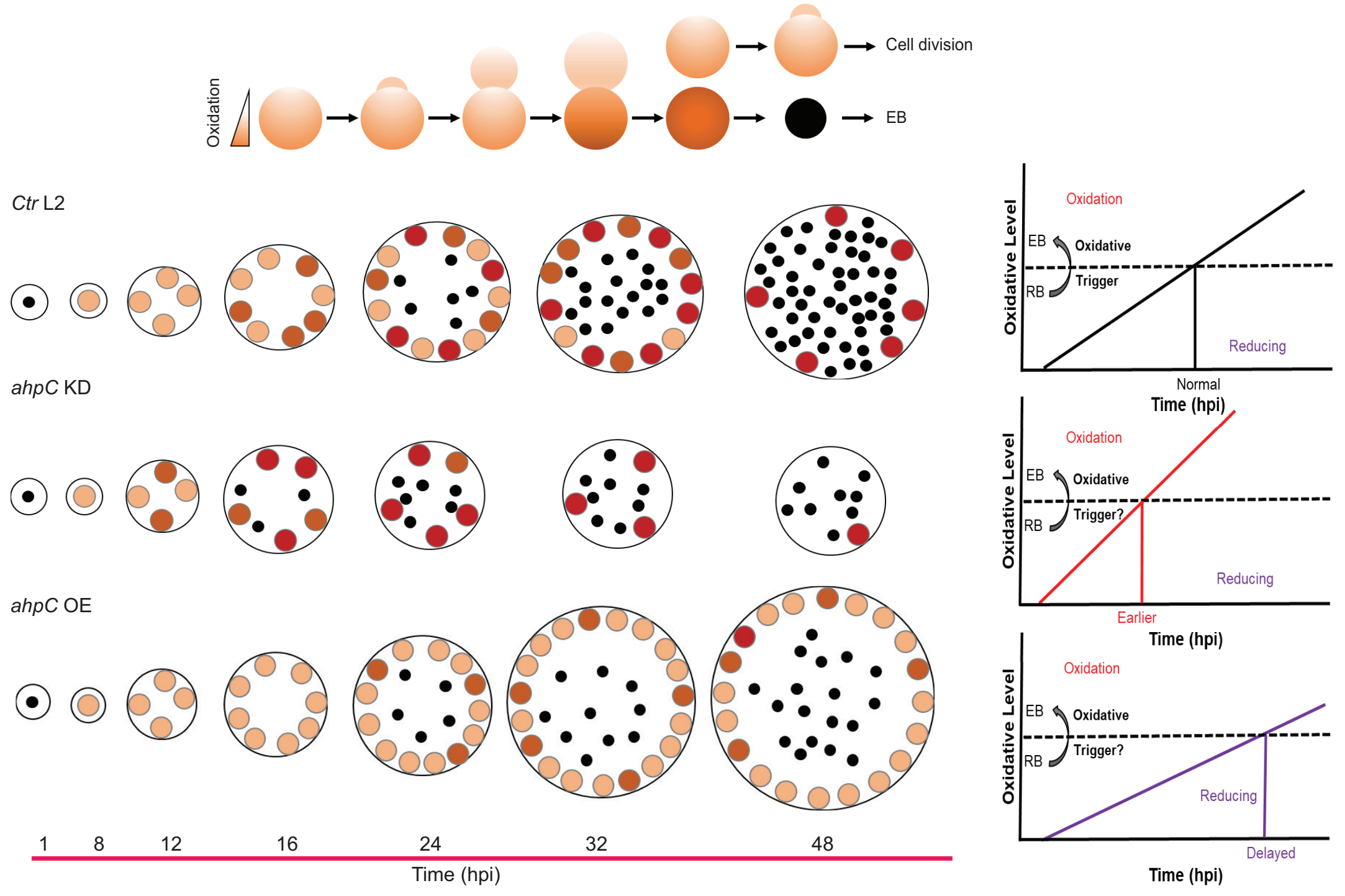
Oxidation
Cell division
EB
Ctr L2
ahpC KD
ahpC OE
1
8
12
16
24
32
48
Time (hpi)
Oxidative Level
Oxidation
EB
Oxidative
Trigger
RB
Reducing
Normal
Time (hpi)
Oxidative Level
Oxidation
EB
Oxidative
Trigger?
RB
Reducing
Earlier
Time (hpi)
Oxidative Level
Oxidation
EB
Oxidative
Trigger?
RB
Reducing
Delayed
Time (hpi)